Title:
A gene-expression module in circulating immune cells is associated with cell migration during immune diseases.

Thomas Laurent*[1], Debajyoti Sinha*[1], Cynthia Fourgeux[1], Thibault Letellier[2], Simon Ville[1,2], Laurence Bouchet-Delbos[1], Julien Brancherau[1,2], Clarisse Kerleau[2], Sophie Brouard[1], Gilles Blancho[1,2], Magali Giral[1,2], Nicolas Degauque[1], Antoine Roquilly[1,3], Regis Josien[1,2], Richard Danger[1] and Jeremie Poschmann[1,4]

[1]Nantes Université, CHU Nantes, INSERM, Center for Research in Transplantation and Translational Immunology, UMR 1064, ITUN; F-44000, Nantes, France.
[2] CHU Nantes, Nantes Université, Institut de Transplantation Urologie Néphrologie (ITUN), Service de Néphrologie et Immunologie Clinique, 44000 Nantes, France.
[3] Nantes Université, CHU Nantes, INSERM, Anesthesie Réanimation, CIC 1413, F-44000 Nantes, France
[4] Corresponding author (orcid : 0000-0002-9613-5297), 30 Boulevard Jean-Monnet, CR2TI, 44093 Nantes, France, jeremie.poschmann@univ-nantes.fr
[*] contributed equally

Abstract:
Circulating immune cells are critical mediators of the response to inflammation upon recruitment to the tissue but how gene expression state influences recruitment is not well known. Here we report the longitudinal single-cell transcriptome profiling of blood mononuclear cells in patients undergoing kidney transplantation rejection. We identify a gene expression module which is associated to transcriptional regulation, homing and early activation in multiple cell types. The circulating cells expressing this module are reduced in patients undergoing graft rejection. This reduction was confirmed in a pig model of acute kidney transplantation rejection. In connection with this, the module expression drastically increased in the kidney grafts undergoing rejection indicating a preferential recruitment of cells highly expressing this module. We identify the receptor CXCR4 within the module and its ligand CXCL12 expressed in the graft as a likely recruitment mechanism between circulating cells and the tissue. We then explore publicly available transcriptomics data in circulating cells and show that this module is generally expressed in healthy individuals and more importantly is associated with the response to infection, including SARS Covid-19. Moreover, we find that module expression is predictive of immune mediated diseases. In summary, we find a gene expression module in circulating immune cells which enables preferential recruitment to inflamed tissues to mediate effector function.

Introduction:

Circulating immune cells are critical to be recruited to the site of inflammation, infection, and cancer. This compartment and particularly the peripheral blood mononuclear cells (PBMCs) thus offer an attractive resource for precision medicine as in a single experiment, diverse cell types, including the $CD4^+$ T cells, $CD8^+$ T cells, B cells, NK cells and monocytes are profiled. Especially since the introduction of single cell RNA-seq (scRNA-seq), profiling PBMCs has been highly successful in identifying gene expression signatures and cell-types associated with immune-related diseases[1–4]. For example, a monocyte signature associated with sepsis was discovered in circulating cells [1]. Recently, a study on systemic lupus erythematosus revealed gene expression changes with disease state and genetic variation [2]. In addition, distinct Covid-19 studies revealed signatures associated to infection and disease severity in blood [5,6].

Transcriptomics profiling enables the characterization of genes groups (i.e., modules) which perform critical cellular functions such as maintaining a cell identity, homeostasis & metabolism and respond to external signals. Notably, in circulating immune cells we have previously shown that monocytes express a gene module associated with Herpes Simplex virus reactivation after traumatic brain injury [7]. While gene expression programs of circulating immune cells are likely to be distinct from the same cells which migrated into the tissue, identifying modules in circulating cells may reveal early immune activation programs or modules associated with homing and migration. For example, in a previous study we identified large gene regulatory and gene expression alterations in circulating monocytes during active Tuberculosis which improved pathogen clearance for these cells [8].

Leveraging on scRNA-seq and the availability of recent module identification approaches tailored for single cell transcriptomics [9] we aimed to identify gene expression programs associated with kidney transplantation rejection. Currently, rejection status is monitored via clinical practice via blood and urine metabolites like creatinine to assess the renal function and then validated via pathology analysis of kidney biopsies [10]. But metabolite monitoring is nonspecific to rejection and can be approximative. Pathology analysis of kidney biopsies thus remains the main diagnostic tool with a more reliable result, but even if it is of limited risk for the patients, it is an invasive procedure which can't be performed on a regular basis. Thus identifying gene expression signatures in circulating cells may improve precision medicine diagnostics of kidney rejection [11]. In addition, acute and chronic rejection are characterized by the infiltration of immune cells into the graft, which then mediate the inflammation response in the tissue, causing the rejection of the graft. Blood thus constitutes an easily accessible compartment to identify gene expression modules associated with homing and early activation. Two archetypes of rejection are prominent according to the Banff classification[10], the antibody mediated rejection (ABMR) and T-cell mediated rejection (TCMR), which can also arise in a mixed form. In both cases, immune cell infiltration into the graft occurs via the bloodstream through either donor specific antibodies binding to the graft endothelium in ABMR, or cytokine and homing signals in TCMR[12].

In this study, our aim was to identify putative modules in circulating cells which may be associated to kidney transplantation rejection. We profiled a longitudinal patient cohort consisting of 3 stable patients, 3 TCMR and 3 ABMR patients at 0-month, 3 month and 12 month after transplantation or when rejection occurred. The PBMCs were collected at the same time of graft biopsy, allowing us to characterize relationship of graft rejection status with gene expression modules of peripheral immune cell-types. We identified a module associated with transcriptional regulation and early activation in the blood and used a pig-transplantation model to validate its association with rejection status. Further characterization of this module was carried out in transcriptomics data from over 1500 kidney biopsies revealing a cytokine-receptor interaction between the graft and circulating cells, respectively. Finally, we demonstrate that this module is not specific to graft rejection but is implicated and predictive of a variety of immuno-pathologies.

Results:

Single cell transcriptome analysis of circulating immune cells in a longitudinal kidney transplantation cohort

In order to identify gene expression changes in circulating immune cells during kidney transplantation rejection, we used scRNA-seq on PBMC isolated from 3 patients with stable allograft function (STA) for which no sign of rejection was observed clinically after more than a year of follow-up, 3 antibody mediated rejection (ABMR) patients and 3 T-cell mediated rejection (TCMR) patients (Figure 1A, Table 1). The patients were selected based on their treatment, age, sex, and collection time. (See Table 1).

Table 1: Clinical summary of the cohort composition.

	Name	Patients characteristics					
		Age	Sex	Treatment *	Rejection time (in days)	HLA ** mismatches	Induction Therapy
Batch 1	STA1	35	*Male*	*Tacrolimus, MMF, Corticoids*	–	5	*Depleting*
	TCMR1	70	*Male*	*Tacrolimus, MPA, Corticoids*	244	5	*Depleting*
	ABMR1	51	*Female*	*Tacrolimus, MMF, Corticoids*	374	2	*Depleting*
	TOL1	75	*Male*	–	–	4	*Depleting*
Batch 2	STA2	69	*Male*	*Tacrolimus, MMF, Corticoids*	–	5	*Non – depleting*
	TCMR2	35	*Male*	*Tacrolimus, MPA, Corticoids*	369	3	*Depleting*
	ABMR2	56	*Male*	*Tacrolimus, MPA, Corticoids*	427	4	*Depleting*
	TOL2	45	*Male*	–	–	4	*NA*
Batch 3	STA3	25	*Female*	*Tacrolimus, MPA, Corticoids*	–	5	*Depleting*
	TCMR3	24	*Male*	*Tacrolimus, MMF, Corticoids*	213	3	*Non – depleting*
	ABMR3	61	*Female*	*Tacrolimus, MPA, Corticoids*	365	2	*Depleting*
	TOL3	39	*Female*	–	–	0	*NA*
		Mean Age 48.75	Sex Ratio 0.66				

* Antiproliferative treatments: MMF=Mycophenolate mofetil, MPA=Mycophenolic Acid

** HLA mismatches: number of mismatches on the A, B and DR loci (0-6)

For each patient, three time points were profiled; T0, at the kidney transplantation, T1 at 90-150 days after the transplantation and T2, which was sampled at the time of rejection for ABMR and TCMR or at 1 year for STA patients after transplantation. In addition, PBMCs from 3 kidney transplantation patients who maintained allograft function in the absence of immunosuppression (i.e., operational tolerant (TOL)) were included in the cohort (Table 1).

Rejection status was defined by clinical pathology assessment of kidney biopsies performed at T1 and T2 for all patients. ABMR and TCMR was defined by pathology biopsy assessment at time T2. whereas patients were determined as STA when they which no sign of rejection in biopsies at T1 and

T2. To minimize scRNA-seq-related experimental variation, we performed CITE-seq (Cell Hashing)[13] using hashtag oligo-conjugated antibodies (HTO) to label each patient and time point separately and then pooled 10 samples (1 ABMR, 1 TCMR and 1 STA patient across T0, T1 & T2 and 1 TOL patient) into a single experiment. We thus generated the complete transcriptomic data in three balanced batches (Figure 1B). After removing doublets, data cleaning, normalization, and batch correction we obtained 50,507 cells across the three batches (see Methods). Cells were automatically annotated using Azimuth[14,15] and manually validated for cell-type specific markers (Figure 1C and Supplemental Figure S1A). Cell-type proportions varied minimally between conditions when compared to PBMCs from two separate cohorts of healthy volunteers (HV) from publicly available scRNA-seq data [1,5] (Supplemental Figure S1B). For example, NK cells were significantly decreased in the stable and rejection conditions as compared to HV. However, we note that there were also significant differences in the HV (e.g., CD14 and CD16 monocytes) from the two distinct cohorts indicating that this may be due to experimental variation and thus may not be biologically meaningful. We then inspected the distribution of cells across patients and by time points (Supplemental Figure S1C) and across disease states (Figure 1D). Neither of these variables formed unique clusters suggesting that the clusters were driven by cell-type specific expression rather than by condition or cellular states as was also observed in other PBMC studies in patient cohorts [1,2,5]. We then explored whether the clusters were affected by merging the three experimental batches (Figure 1E). As no batch effects were visible by eye we precisely quantified possible batch effects using the KBET metric which evaluates whether cells from different batches are forming neighborhoods (i.e., clusters) (Supplemental Figure S1D)[16]. The acceptance rate of the KBET for the complete data set was 0.969, indicating that batch integration was successful. In summary, the pooling strategy and subsequent bioinformatics analysis resulted in a robust dataset of 50,507 cells to be analyzed for time and disease state specific gene expression.

Gene co-expression analysis identifies a module associated to rejection state

To identify modules, ie. co-expressed groups of genes we used gene co-expression analysis across all three batches independently (Figure 2A). This approach was chosen to avoid potential signal alterations induced during the batch correction step. We applied consensus non-negative matrix factorization (cNMF)[9] to identify gene expression programs which may either be associated to cell-type specific gene expression programs or to cellular activity (see methods). Nine overlapping modules were identified which were evenly distributed across the three batches (Figure 2B, Supplemental Figure 2A). These modules mostly revealed cell-type specific expressions, notably three of these modules were associated to monocytes (Mod_1-Mod_3), and two modules were mostly expressed in a specific cell type such as B cells and pDC cells (Mod_4 and Mod_5 respectively) (Figure 2C). Three modules were enriched for the CD4 & CD8 T lymphocytes (Mod_6) and/or NK cells (Mod_7, Mod_8, Figure 2C). Interestingly, the Mod_9 was expressed in all cell types, but with notable higher expression in B cells, T cells, pDCs and NK cells as revealed by its module score (Figure 2C, Figure 2D).

Next, we aimed to independently validate the co-expression of the 9 modules (Supplemental file 1). To achieve this we quantified the gene co-expression using the pair-wise Pearson correlation coefficient R. As the module was identified using cNMF, Pearson correlation thus acts as an independent evaluation of gene co-expression. We note that this approach is inherent to weighted gene co-expression analysis (WGCNA), a prominent method to identify modules in bulk and single cell transcriptomics[17]. We compared the average Pearson correlation per cell for each module to the same number of randomly picked genes in the same cells. The eight cell type specific modules showed robust and significant correlation between module genes, and this correlation was strongest in the cell-types to which they were associated (Supplemental figure S2B). The cell-activity module Mod_9 was also significantly correlated in all cell types (Supplemental figure S2C). Of note, randomly chosen genes picked 1000 times revealed a Pearson correlation of 0 in all cell-types indicating that unrelated genes typically do not correlate with each other (Supplemental figure S2B, S2C). Therefore,

the modules identified above are robustly co-expressed, as inferred by the two most prominent module detection methods.

To test whether this cell-activity module or any of the cell-specific modules were associated to disease state, (i.e., rejection or stable) and if it would vary throughout time, we estimated the module score for each cell type and calculated the trend of the module score longitudinally in each cell-type (Figure 2E). A positive or negative slope thus indicates whether a module changes over time across the stable, humoral & cellular rejection. Indeed, Mod1 and Mod2 showed a significant positive trend in both rejection conditions (ABMR and TCMR) but not in the STA condition. Interestingly, the activity module (Mod_9) showed a significant negative trend (regression β value) in the rejection conditions but not in the stable condition in multiple cell types (B cells, CD4 and CD8 T cells and NK cells). Further inspection of this negative trend was carried out by displaying the module score of each patient separately in the form of a combined violin plot (Figure 2F). These module scores show that there was indeed a reduction in ABMR patients, while in TCMR patients the module score followed a U-shape, reduced more during T1 and increased again at T2. Interestingly, the 3 stable patient's module scores remained consistent across time in NK, CD4 and CD8 and B cells. These results signify that Mod_9 expression is associated to rejection state in a time dependent manner.

Discovery of the early activation, transcription factor module (ALARM)

To explore the function of the 61 genes found in Mod_9 we first investigated whether it was enriched for ribosomal, proliferation or cell cycle genes using SEURAT-based list [18]. We did not observe any genes involved in these cellular processes (data not shown). We thus explored the genes within this module by performing gene ontology analysis. Enrichment of the module genes was quantified for molecular function (MF) and biological processes (BP) compared to the combined set of 4000 most variable genes from the three batches (Figure 2G). MF could be associated to 24 genes and was significantly enriched (FDR <0.05) for helicase activity, ubiquitin-like protein binding, RNA catalytic activity, transcription activator activity and ribonucleoprotein binding. The BP (20 genes) was associated to NF-κB signaling, response to peptide and oxidative stress, regulation of RNA metabolic processes and viral gene expression. Of the 61 genes in the module, 56 were annotated in the GSEA database and 30 of these genes were linked to gene ontology enrichment. This indicates that Mod_9 is likely to be involved in multiple molecular functions associated with transcription, mRNA process and ubiquitination. The BP suggested involvement in response to immune conditions (i.e., viral gene expression, NF-κB signaling, oxidative stress). This result was further supported by the 5-fold enrichment of Transcription factor genes in this module (OR: 4.9; Fisher-Test P-value $2.5e^{-5}$), such as the AP-1 complex (*JUN, JUND, FOS*), *REL* (NF-κB subunit), *MAFF* and *NR4A2* (see methods, Supplemental file 1). Further manual examination exposed the early activation marker CD69, a cell surface type II lectin. This receptor was described to be rapidly expressed at the membrane in T cells upon TCR activation[19]. In addition, CD69 has been described as a marker of tissue retention of T cells [20–22]. Interestingly, *CD69* gene promoter is controlled by AP-1 TF complex and NF-κB, both of which are also members of this module[23,24]. We also found the cell surface marker CXCR4 in this module, a chemokine receptor known to play a role in recruiting CXCR4 positive cells to the kidney after an ischemic injury via the chemokine CXCL12[25]. The role of the CXCR4/CXCL12 axis in kidney rejection is still unclear[26] but an elevated expression of CXCL12 has been described in chronic kidney rejection[27] suggesting it may act as a chemotactic signal to recruit immune cells in the inflamed tissues. In summary, the Mod_9 module comprises genes implicated in the response to stress, mRNA processing, early activation, and tissue-homing. For clarity, we named this module ALARM, which stands for for eArLy activation trAnscription factoR Module.

Circulating ALARM cells are recruited to the graft during acute graft rejection in a pig kidney transplantation model

We found that circulating cells expressing ALARM are altered in ABMR and TCMR in a timely fashion (Figure 2). To independently validate this observation, i.e., whether ALARM high expressing cells are

depleted in the circulation during kidney transplantation rejection, we took advantage of an acute rejection pig kidney transplantation model (Figure 3A). We decided to use a pig kidney transplantation model as they share anatomical, physiological and genetic similarities to human and offer the advantage to have well defined swine leukocyte antigen (SLA) genotypes [28]. Two SLA-mismatched pigs were subjected to kidney transplantation, keeping one of their own kidneys (see methods). This model typically results in an acute TCMR within a few days after transplantation, as no immunosuppressive treatment is given (Figure 3A). Kidney biopsies and PBMCs were collected daily before and after the transplantation. Microscopical analysis of the biopsies at D2, D4 and D6 indicated a time-dependent infiltration of immune cells, culminating at day 6 (Figure 3B). This infiltration was quantified in three areas (excluding glomeruli) of each biopsy time point (see methods, Supplemental Figure S3A). Cell counts drastically increased from day 2 to D6, indicating a continuous immune cell accumulation over time (Figure 3C). We noted that the second pig did not display any signs of rejection, possibly due to early arterial ischemia of the transplanted kidney and it was thus discarded from the subsequent analysis. PBMCs collected at D0, D2, D4 and D6, were pooled in a single scRNA-seq experiment (see methods), resulting in a total of 4,411 annotated cells across cell-types and time-points (Figure 3D and Supplemental figure S3B). We found that cellular proportions within the PBMC compartment drastically changed from D0 to D2, characterized by a drastic increase in monocyte proportions concomitant with a reduction of B, CD4+ and CD8+ T cells (Figure 3E). This suggests that the lymphocytes are rapidly recruited to the kidney graft and accumulate there, as demonstrated by the cellular invasion observed in the biopsies at the same time (Figure 3C). To test whether the decline of blood lymphocytes is accompanied by a reduction of ALARM high expressing cells, we quantified ALARM expression across the time-points in CD4+, CD8+, B cells and NK cells (Figure 3F). Interestingly, as soon as D2 the levels of ALARM expression drastically decreased when compared to before transplantation (D0) and remained low in the blood until sacrifice of the animal (D6). Taken together, this controlled time-course experiment reveals a drastic immune cell infiltration in the graft associated with the depletion of ALARM high expressing cells in the circulation. This result mirrors the reduction of circulating ALARM cells observed during the kidney transplantation rejection in the human cohort (Figure 2). It is thus probable that ALARM high expressing cells are readily circulating in the healthy condition. Upon the kidney graft transplantation ALARM high expressing cells are then preferentially recruited to the organ to mediate the immune response.

ALARM gene expression increases in kidney grafts undergoing rejection

To further support the hypothesis that ALARM high-expressing cells are recruited to the graft during rejection from the bloodstream, we evaluated the expression of ALARM genes in graft biopsies from kidney transplantation patients. For this, we used a previously published Canadian transcriptomics analysis of 569 transplant biopsies collected from 13 clinical sites and with a patient classification of STA, TCMR, ABMR and mixed rejection (TCMR and ABMR)[29]. In parallel, we exploited a second similar Belgian transcriptomics study performed on kidney biopsies in 224 patients who were either stable (168 patients) or undergoing ABMR[30]. After precleaning and QC controls of the available microarray data (Methods), we quantified the ALARM gene expression in each cohort separately (Figure 4A). The ALARM score was consistently and significantly increased in the three rejections compared to the stable biopsies. Similarly, in the second study ABMR samples, independently of the presence of donor specific antibodies, were significantly increased for ALARM expression. Heatmap analysis of the ALARM genes ranked by expression, further revealed that this score is driven by the upregulation of a large fraction of the ALARM genes, including *CD69*, *CXCR4*, *JUN* and *IRF1* in both cohorts (Figure 4B). Quantification of the ALARM module across rejection and stable revealed a significant upregulation of ALARM expression in both data sets (Figure 4C). These results indicate that ALARM genes are significantly increased during graft rejection across over 793 biopsies in two distinct studies. Given that graft rejection is defined by immune cell infiltration and that circulating ALARM high cells are depleted at the same time, it is possible that ALARM high cells are preferentially recruited to the graft to mediate the rejection.

To investigate how circulating cells could be preferentially recruited to the graft, we explored the cytokine expression in the graft and receptor expression in the circulating cell subsets. We first identified all possible ligand-receptor pairs and then tested whether these pairs were differentially expressed between rejection and stable status. We found 10 differentially expressed cytokines in the graft pairing with 7 receptors upregulated in circulating immune cells in both cohorts independently (Figure 4D). The most prominent receptor was CXCR4, expressed in CD4, NK, CD8 and B cells. As mentioned above, CXCR4 is a member of ALARM genes, indicating a likely mechanism of signaling from the graft via CXCL12 and recruitment of ALARM cells expressing *CXCR4*. This cytokine receptor pair has been previously described as a homing mechanism in various distinct tissues, such as bone marrow[31,32] and in cancer[33]. To test the relationship of this interaction, we quantified *CXCL12* expression in the graft biopsies stratified by ALARM expression (low (<25%), mid (25-75%), high (>75%)) and found that there was a significant increase in CXCL12 expression in the ALARM high group in both cohorts (Figure 4E). In summary, these results show that ALARM is increased during rejection in the graft, which strengthens the notion that circulating cells with high ALARM expression are preferentially recruited to the kidney graft via the homing signaling axis of CXCL12 and CXCR4.

ALARM is expressed in healthy individuals and variation is associated with infectious disease

So far, the role of ALARM cells has been explored in the context of kidney rejection and stable kidney transplantation patients which are both under immune suppressive treatment (see table 1). We thus investigated whether this module is generally expressed across a healthy population. For this we explored a publicly available scRNA-seq data set of ~25,000 PBMC from 45 healthy volunteers (HV) for ALARM expression [34]. The data was generated from the *LifeLines DEEP* cohort in Netherland, ranges in age from 20 to 79 and contained 46,6% female individuals and was described to be healthy time of collection as estimated by two general practitioner visits [35]. ALARM expression was prominent in all cell types as shown by its module score suggesting that ALARM is generally expressed in HV (Figure 5A). We note that age and sex did not result a significantly different expression of the ALARM (supplemental figure S5B). If this module is generally expressed in HV, we next asked whether it may be involved in other disease conditions than transplantation rejection, but which implicate the recruitment of circulating immune cells to specific tissues. To test this hypothesis, we exploited a publicly available scRNA-seq data on PBMCs in which healthy individuals were intravenously injected with the endotoxin lipopolysaccharide (LPS), a component of the cell wall of Gram-negative bacteria [5]. LPS in the bloodstream causes an immediate systemic release of a variety of inflammatory mediators, a fever and a rapid but transient leukopenia [36,37]. This experiment is thought to mimic an acute systemic inflammatory response (SIRS) [5], and thus provides an ideal proxy of how ALARM expressing cells are responding to LPS-induced SIRS. We used the preprocessed available scRNA-seq data which contained the 0-time point (10 HV), 90 minutes (6 HV) and 10h after the LPS injection (6 HV) and first evaluated how the cellular proportions changed over time. We measured the ALARM score in the three conditions across the CD4, CD8, NK and B cells (Figure 5A). There was rapid and significant reduction of ALARM high expressing cells as soon as 90 minutes and which further decreased until 10h after the LPS injection. This decrease was continuous within three individuals for which both timepoints were available, indicating that ALARM cells are reduced in a time dependent manner (Figure 5C). This drastic change of ALARM expression in such a short time frame suggests that cells which highly express this module rapidly egress from circulation, directly contributing to the transient leukopenia observed upon LPS injection. This is also consistent with the transient leukopenia associated to LPS i.v. injection. Furthermore, this response to LPS which is thought to be initiated via TLR4 receptor signaling expressed on circulating monocytes [38,39] signifies that ALARM is not solely implicated in transplantation rejection or kidney immune cell invasion but appears to also be involved in the inflammatory response to endotoxin.

Next, we investigated how ALARM may regulate when the site of inflammation is localized to a single organ as in urinary tract infection. For this we explored a publicly available PBMC scRNA-seq dataset which contained patients with leukocyte infiltrating urinary tract infection (UTI). We chose this condition as the data was generated on patients which presented a localized infection with infiltrating leukocytes. The study also provided results of HV and sepsis patients, notably patients with bacteremia, i.e. bacterial presence in the blood. [1] (Figure 5D). The bacteremia patients were thus also used for comparison since this condition reflects a generalized or systemic infection which is distinct from a localized infection such as UTI (Figure 5D). Interestingly, we found that ALARM expression was reduced in circulating cells in UTI patients (except B cells), consistent with the recruitment of leukocytes to the tissue. In contrast, in patients with bacteremia, the ALARM cells accumulated in the circulation, indicating that under this condition ALARM expressing cells may not be recruited to a specific tissue. This contrasted with the response to LPS i.v. which is also thought to engender a systemic response (see discussion).
To further explore the role of ALARM in response to localized infection, we analyzed two scRNA-seq datasets generated from Covid-19 patients [5,40]. The aim was to explore the dynamics of ALARM cells in the circulation in comparison to the lung. For this, we compared ALARM expression in PBMCs with ALARM expression in broncho-alveolar lavage fluid (BALF). The two separate original studies stratified the patients by healthy, moderate, and severe Covid-19 disease and we used this stratification to compare the ALARM module expression in the blood (PBMC) and in the lung (BALF) (upper panel figure 5E). The ALARM cells diminished according to disease severity (T, B, Mono, but not NK) in the blood stream. This reduction was concomitant with an increase of ALARM high cells in the lung suggesting that ALARM cells are migrating to the site of infection. We note that the cell-type specific modules did not change between disease state and between blood and lung (lower panel, figure 5E) indicating that the similar cell types were analyzed and that the cell-type specific modules were not related to disease state. Collectively these results show that ALARM displays a normal distribution of expression across healthy individuals and changes in response to distinct disease states (bacterial, viral, kidney rejection). It is noteworthy that expression alterations of this module are apparent in distinct cell types depending on the disease conditions.

Disease classification of ALARM in immune mediated diseases

The above results suggest that ALARM expression changes are associated to immune diseases, likely via the recruitment of circulating immune cells to the site of inflammation. It may thus be possible that the ALARM genes could be used as predictors for immune disease classification. The rationale is that if ALARM genes are relevant for a precise disease state they would be strong predictors to classify healthy from disease [41]. To investigate this hypothesis, we analyzed 10 immune-mediated diseases with distinct tissue tropisms (Supplemental Figure 6A). Out of these 10 diseases, systemic lupus erythematosus (SLE), Sjogren syndrome and Anti-neutrophil cytoplasmic antibody-associated vasculitis (ANCA) are known to favor the kidney among other organs. In contrast, mixed connective tissue disease and systemic sclerosis rather favor the connective tissues and rheumatoid arthritis targets the joints. Thus, we aimed to test whether ALARM genes are good classifiers of disease vs healthy condition and whether the classification of disease state varies depending on the tissue tropism. This was possible thanks to a large bulk RNA-seq dataset comprising 28 circulating immune cell-types which included 337 patients across 10 immune mediated diseases and 79 healthy controls [42] (Supplemental figure S6A). We evaluated total gene expression using UMAP of this data set (Figure 6A) and found that ALARM module expression was present in all major cell types (Figure 6B). To test the discriminative ability of the ALARM module we then devised a classification pipeline comparing disease state (all 10 immune diseases) vs healthy using logistic regression (Figure 6C). As in the data set there were transcriptomics data from 28 cell types available, we focused on B cells, T cells, NK and Monocytes by regrouping their respective sub cell types together (see Figure 6A).

We then generated an ALARM gene classification model compared it to two other models. The first one using the most variable genes (coefficient of variation (CV^2), see methods) and the second model was based on genes in cell type identity modules (see figure 2). The rationale for using CV^2 gene selection was to use an independent gene selection process which is more predictive than random gene selection. We compared the prediction performance of the three models using the F-1 score as it gives equal weight to precision and recall (Figure 6D, F1 score). Interestingly, the ALARM genes were the best predictors for CD8, Monocytes and NK cells and were similar in performance to the cell type specific modules of CD4 and B cells. To account for possible imbalances in the numbers of disease and control samples we also computed the Cohen's Kappa score (Supplemental Figure S6B). The results were consistent with the F-scores. Of note, the CV^2 gene selection approach was less predictive in all cell types (figure 6D and Supplemental S6B).
To evaluate whether the ALARM module was prominent for any specific cell sub types within the major cell types (e.g., CD4 memory cells vs CD 4 cells) we estimated disease classification performance of the ALARM module separately for each sub type. Predictability as estimated by F1 score remained robust when each subtype was analyzed separately in comparison to the CV^2 method (Figure 6E). We note that in certain subtypes there were too few samples to compute an accurate Kappa score (Supplemental figure S6C). Nevertheless, this result indicates that ALARM was found to be relevant in all the subtypes analyzed.
Next, we evaluated whether each of the 10 immune mediated diseases could be individually classified from healthy (Figure 6F). The best classification ability of ALARM was found for Mixed connective tissue disease, rheumatoid arthritis, Sjogren's syndrome, SLE and Takayasu's Arteritis. This indicates that ALARM genes are not specifically predictive for tissue tropism but appear to be relevant independently of the targeted tissue. In most cases ALARM outperformed the CV^2 feature selection suggesting that ALARM genes are likely to be implicated in their disease etiology. In summary, this comprehensive classification analysis indicates that ALARM genes are strong predictors of disease state across the majority of circulating immune cells and within the 10 immune related diseases.

ALARM is enriched for genetic disease associations

Since the ALARM genes are strong predictors of immune mediated disease and its general role within multiple cell-types and across multiple infections, immune related and autoimmune diseases it is likely that ALARM is enriched for genes known to be associated to diseases. To test this, we exploited the DisGeNET database[43] which provides a comprehensive compilation of published and curated human gene disease associations (GDAs) from repositories including Mendelian, complex and environmental diseases and enables enrichment analysis of such GDAs. Notably, we found that 24 out of the 61 ALARM genes (39%) were associated with a disease. To estimate the probability of this occurring by chance, we compared this to random sampling of 61 genes and their quantification of GDAs (Supplemental Figure S6D permutation). The probability of reaching 40 % of genes or more was below > 0.001, indicating that ALARM genes are highly enriched for GDAs.
Next, we tested whether the ALARM genes were enriched for diseases associations (Figure 6G). The top three disease categories enriched for GDAs were Juvenile arthritis, Hodgkin disease and polyarthritis comprising by themselves distinct 13 genes. This genetic enrichment analysis indicates that ALARM is also genetically connected to disease state. In summary, ALARM is a strong classifier and genetically linked to immune disease and thus is likely to play a general role in multiple immune mediated diseases.

Discussion:

In this study, we gathered a cohort of matching ABMR, TCMR and stable patients and generated a comprehensive scRNA-seq atlas of circulating immune cells across time and conditions. We then identified multiple gene co-expression modules across batches. Five out of nine modules were nearly related to a single cell-type while three were expressed in closely related cells (CD4+, CD8+ and NK

cells) and only the ALARM module was prominent in multiple cell-types. The observation that most cell-type specific modules were discovered was also described by Kotliar et al., [9] in which they distinguish between identity (i.e., cell-type specific) gene expression programs (GEP) and activity GEPs. It is possible that cell-type specific co-expressed genes are better detected as they show a greater coherence within a well-defined group of cells. This is also notable in the presented data as the module scores show less variance than the ALARM module. Nevertheless, cell-type specific gene expression may not necessarily imply that it remains constant across conditions. For example, we noted that some cell type specific modules were associated to disease state (figure 2E), notably the NK cell and monocyte specific modules were increased during rejection. It is also possible that because of the relatively low number of genes per cell detected when compared to bulk transcriptomics, cell identity programs are preferentially detected, and more subtle condition specific modules are not robustly detected. Indeed, while cNMF revealed additional modules in the separate batches, only the ALARM module was consistently identified across the three batches.

The ALARM genes were found to be highly enriched for transcription factors and gene ontology pathways associated with the gene expression machinery including transcription, mRNA processing and ubiquitination. Prominent transcription factors included the AP-1 complex and the NFKB subunit REL which are both associated with stress responses and inflammation. The membership of CD69 in the ALARM module also suggests a role of stress response. CD69 is a classical early activation marker of lymphocytes, as demonstrated by its rapid display on the surface of T cells after TCR stimulation[44]. In addition, CD69 is also known to be a tissue retention marker as it is expressed on resident memory T cells in distinct tissues. In blood, this gene has been associated with chronic inflammation in various diseases including rheumatoid arthritis [45] and systemic lupus erythematosus [46]. Concomitant with this, CD69 protein expression is increased on infiltrated immune cells at the site of inflammation in immune mediated diseases including systemic sclerosis, rheumatoid arthritis, systemic lupus erythematosus[44]. The membership of CD69 in this module thus indicates that this module is important to prepare circulating cells T cells for TCR stimulation and for tissue retention once moved into a tissue, i.e., to become T resident effector cells. This notion is also consistent with the increased expression of the ALARM module in the kidney biopsy transcriptomics data (Figure 4).

The cytokine receptor CXCR4 was also identified in this module. CXCR4 is predominantly expressed by lymphocytes as well as monocytes and through which the CXCL12 ligand promotes chemotaxis to tissues via a concentration gradient [47]. CXCL12 is expressed in multiple tissues including the kidney and is altered during pathophysiological responses including immune diseases. Indeed, an alteration of CXCL12 expression was observed in the kidney transplantation biopsies and this increase was associated to elevated ALARM gene expression in the tissue (Figure 4E). It is possible that the CXCR4-CXCL12 axis contributes to the recruitment of ALARM expressing cells in the case of kidney transplantation rejection and other immune diseases. This is also consistent with the observation that cells expressing the ALARM module decrease in the circulation during kidney graft rejection. This observation was confirmed by both, transcriptomics and histological studies of pig as well as transcriptomics in human kidney biopsies, thus, via CXCR4-CXCL12 leading ALARM cells to infiltrate the tissues during rejection.

This CXCR4-CXCL12 axis also highlights the notion that the ALARM module is not necessarily specific to transplantation rejection or the kidney. Indeed, reanalysis of circulating immune cells from publicly available scRNA-seq data showed that the ALARM module was expressed in 45 unrelated healthy individuals [34] and showed significant alteration between distinct pathological conditions (Figure 5). First, the ALARM response to LPS iv injection in healthy individuals revealed that it is time-dependent, illustrated by a gradual decrease of ALARM cells within the same individuals over time. Second, there was a significant difference between ALARM cells depending on the location of the pathological condition. ALARM cells were shown to be decreased in response to kidney rejection, in response to leukocyte infiltrating UTI and Covid-19 infection of the lung highlighting the role of ALARM in the recruitment of cells to the site of inflammation and infection. This was further supported by bacteremia sepsis, a state of systemic inflammation in which ALARM cells were increased in the blood. While LPS i.v. injection and bacteremia induce both a systemic immune

response, the former is associated is essentially an endotoxemia response associated to a transient leukopenia[36,37] while the latter is a complex and heterogeneous condition that involves multiple factors beyond LPS, such as pathogen virulence, host susceptibility, and coexisting medical conditions. It thus makes sense that the leukopenia is associated to the decrease of ALARM, while in bacteremia ALARM expression is increased. Third, ALARM cells showed a gradually measurable response to disease severity. This notion was observed by combining two distinct and complementary Covid-19 datasets one of which was collected on BALF, and which had stratified their patients according to disease severity. ALARM cells decreased in response to severity in the blood with a corresponding increase in the lung.

Fourth, we collected several lines of evidence suggesting that ALARM cells are indeed recruited to the site of inflammation and/or infection. During acute rejection induced in the pig model there was a rapid infiltration of leukocytes concomitant with the reduction of ALARM cells in the blood. The analysis of >800 kidney biopsies revealed an increase of ALARM gene expression during kidney transplant rejection. Similarly, the recruitment of ALARM cells to the lung was observed during Covid-19 lung infection. We thus propose a model in which ALARM expression priorities the infiltration capacity of each circulating cell (see figure 8 model). This model has wide ranging consequences in precision medicine as blocking of ALARM cells to the site of inflammation in the case of kidney rejection may prevent further organ damage or attenuate the immune response in the case of Covid-19 lung infection. It may also be useful to predict disease state as we have shown in figure 6. ALARM was a strong classifier of immune disease when compared to healthy individuals. The importance of ALARM was independently demonstrated by its enrichment for genes mutated in notably juvenile and poly- arthritis. Further investigation is however required to test the specificity of disease detection or whether ALARM is merely a response to inflammatory state in the circulation.

There are several limitations of this study, first it is based on gene transcription and thus remains to be explored for protein expression, however this is difficult to achieve at single cell resolution and we are not aware of any gene co-expression modules estimated at the protein level. While the module expression was shown to be low in the blood and high in the kidney tissue during rejection, the direct evidence of the recruitment of these cells to the tissue remains to be confirmed. For this, notably trans well assays may be suitable for demonstrating the preferential recruitment of ALARM cells via the CXCL12-CXCR4 axis. A further limitation is that as of now we do not have a protein surface marker panel that could be associated to cells with high or low ALARM expression. Such markers would enable the purification of ALARM cells enabling further molecular and cellular characterization. Markers would also allow the targeted modulation of the recruitment of ALARM cells to the graft or during Covid19 as well as other immune mediated diseases may thus impact disease severity. Nevertheless, our study remains important in terms of precision medicine, highlighting the discovery of the ALARM which expression enables cells to be preferentially recruited to the inflamed tissue. This notion is likely to open novel strategies of disease monitoring and disease intervention.

Methods:

1. Study of kidney transplant patients

Kidney transplantation patients

The PBMC samples used in this study (see table 1) were obtained from the DIVAT biocollection (CNIL agreement n°891735, Réseau DIVAT: 10.16.618). Every patient included in the study was enrolled in the DIVAT biocollection following their informed consent. The PBMC from patients were isolated

from kidney transplantation biopsies, frozen with DMSO 10% and stored in liquid nitrogen at the Centre de Ressources Biologiques (CRB, CHU Nantes, France).

Cell preparation

Frozen PBMC samples were rapidly thawed and resuspended in complete Roswell Park Memorial Institute (RPMI) 1640 media (Invitrogen, Carlsbad, CA) with 5% FBS, pre-heated at 37°C.

Following washing steps in PBS+0.04%BSA, cell pellets were resuspended in 200µL FACS buffer (1X PBS supplemented with 2mM EDTA, 2% FBS) in which dead cells were labelled by adding 0.1 µg/mL DAPI (Invitrogen, Carlsbad, CA). Cells were filtered on 70 µm cell strainer and living cells were then sorted using a Fluorescence-activated cell sorting (FACS) Aria II cell sorter (BD Biosciences, Mountain View, CA). We used the same method as previously described for single cell RNAseq[48,49]. One million cells were kept for each sample and resuspended in 100µL of staining buffer (PBS,2%BSA,0.01% Tween) according to the cell hashing protocol[13] recommendations. Cells were incubated for 10 min with 10µL of human Fc blocking reagent. Each sample was then mixed with 1uL of a specific TotalSeq-A hashtag antibody (BioLegend, San Diego, CA) and incubated on ice for 30 min. Following 3 washing steps with the staining buffer, cells were counted and their viability measured using an ADAM-MC automatic cell counter (NanoEntek, Seoul,South Korea) to ensure a viability above the recommended 70%. All the samples were pooled at an equal cell concentration in a single vial, centrifugated and resuspended in PBS to obtain a concentration of 700 cells/µL, to match the targeted cell recovery of 32,000 cells. Encapsulation of single cells was performed on a 10XChromium (10X Genomics, San Francisco, CA) with the Chromium Single Cell 3 Library and Next GEM reagent kit v3. The libraries were sequenced twice for each of the three experiments on the NovaSeq 6000 (Illumina, San Diego, CA) with S1 flow cells. The sequenced libraries were aligned to the GRCh38-2020-A reference genome with CellRanger v5.0.0 (10X Genomics, San Francisco, CA). The scRNA-seq was performed in 3 different experiments following the same protocol. Each experiment included longitudinal samples from three patients (one stable patient, one humoral rejection and one cellular rejection) as well as one late sample of a tolerant patient.

Method demultiplexing and Seurat analysis

The count matrices were analyzed in R 4.0.3 using the Seurat R package (v4.0.2, Satija Lab[14]). Each experiment was first processed separately, with the same workflow. First, following the standard workflow recommendations, cells with less than 200 unique feature counts were removed (potential empty droplets). Cells with a percentage of mitochondrial genes greater than 15% were excluded as it results from mitochondria degradation from dead or dying cells. The hashing antibody sequences were then collected to demultiplex and assign each cell to its sample using the MULTIseqDemux function. Cells with too little labels information were called “Negative” while cells with a high count of two or more different oligo-conjugated antibody sequences were called “Doublets”. Only cells with a unique HTO were kept for downstream analysis. Singlet cells were annotated automatically with the Azimuth workflow within Seurat, by mapping the query cells on an annotated reference of 162,000 PBMC measured with 228 antibodies[15].

All the runs were then merged in a single Seurat object. Doublets and contaminant cells to exclude were selected by identifying cells co-expressing marker genes from distinct cell types. After normalization of the global object, the 2,000 most variable genes in the data were selected to compute the correction using the reciprocal principal component analysis (RPCA). The final annotated and corrected object gathering the 12 patients was composed of 50,507 cells.

Gene Module Identification

Consensus Non-Negative Matrix Factorization (cNMF)[9] was used to decompose the cell vs gene expression matrix into cell vs module and usage vs gene low-rank matrices. Non-Negative Matrix Factorization is a stochastic method and therefore it was run with 200 NMF replicates to find a consensus robust factorization. For each batch, the top 2000 over dispersed genes were selected as input to the cNMF run. Different K values (7 to 14) were explored to determine the optimal number of modules. For each K, the *stability* and *error* metrics were examined. The best K was chosen such that the error was minimum, and the stability was maximum. Each batch was independently

processed to mitigate batch effects from the three different runs. For the three batches, the optimal number of modules (K) were 14, 11 and 13.

Module filtering: All modules from the three batches were collated and hierarchical clustering was performed to identify matching modules. Jaccard similarity score was used to define the similarity between two modules. Finally, only those clusters were retained that could represent all three batches. In this way, nine consistent modules were identified. A unique geneset was determined for each consistent cluster by intersecting the top-ranking 200 genes from the modules. The threshold was achieved by observing a scree plot of input number of genes vs the number of genes after intersection.

Module association: The genes in the module were examined for a module to be associated with a known cell type. The modules containing marker genes were associated with their respective cell type; for example, the module with MS4A1 and CD79A genes was associated with B cells. However, one of the modules (Module 9, later named as the ALARM module) could not be associated with a known cell type as it did not contain cell type specific markers and was well expressed in multiple cell types.

UCell module score

The enrichment of a particular set of genes in an individual cell was measured with the UCell[51] module score. The score is calculated using the Mann-Whitney U statistic, which compares the expression levels of the module genes relative to the total gene expression of the cell. The U-statistic outcome is then normalized between 0 to 1 to produce the UCell score.

Regression analysis

Change in the module score (μ) along time (τ) for each condition was modelled with linear regression method. The 'lm()' function from R *stats* package was used to fit a distinct model $\mu \sim \tau$, per celltype within the group of Stable, ABMR and TCMR individuals. A positive slope indicated that the module score increased with time.

Gene Ontology analysis

The gene ontology (GO) functional enrichment of the ALARM module gene list was performed using the R package WebGestaltR (v0.4.4) for Biological Process (BP) and Molecular function (MF) annotation. P-value are obtained with the hypergeometric test for ORA (Over-Representation Analysis). As background dataset for enrichment the top 2000 variable genes from each run were merged and used.

Transcription factor enrichment analysis

To test for enrichment of transcription factors in the ALARM module, GSEA molecular signature database was used to count the transcription factors gene family in the module and in the background dataset used for gene ontology analysis. Fisher exact test was used to calculate the P-value and enrichment of transcription factors in the ALARM module.

2. Allogeneic kidney rejection model in pig

Animal model

The study protocol was approved by the French Ministry of Higher Education, Research and Innovation (APAFiS #30136). The experiment was performed on 60 to 80kg male pigs (*Sus scrofa*). Test card with pre-applied antibodies from Serafol (Berlin, Germany) were used to identify the pigs' ABO blood groups. The alloreactivity was performed by mixed lymphocyte reaction assay between donor and recipient. The donor pig was selected from a different breed as inbred pigs might escape rejection. Donor and recipients blood groups were ensured to be compatible to avoid hyper-acute rejection, and mixed lymphocyte reaction assays were positive thus proving their alloreactivity.

Allogeneic transplantation

Unilateral nephrectomies were performed on two recipient pigs under general anesthesia with a premedication by Zolazepam/Tiletamine (Zoletil ® Virbac, Carros, France) 15 mg/kg IM, before intubation and a maintained ventilation with a mixture of 49% oxygen, 49% nitrous oxide and 2% isoflurane. The two kidneys from a third donor pig were harvested in the same operating time. The two recipient pigs received one collected kidney each for an orthotopic transplantation. During

surgery, a central venous catheter (CVC) was inserted into the internal jugular vein for hydration and medication. Post-operative analgesia was performed every day with intravenous injections of Nalbuphine (Nubain ®, Mylan, Canonsburg, Pennsylvania) and Paracetamol at a dose of 25 mg/kg. Prophylactic antimicrobial therapy was conducted with Cefazolin 1 g (Cefovet ®, Dopharma, Ancenis, France).

PBMC collection in Pig model

Blood samples were collected daily through the CVC and frozen in a CoolCell® container (Corning ®, Corning, NY, USA) at -80°C following the PBMC isolation. Kidney transplant biopsies were collected daily using automated biopsy needles of 16 gauges under ultrasound guidance while pigs were sedated by Zolazepam/Tiletamine and locally anesthetized with Lidocaine. Kidney samples were then placed in cryovials with 1mL fetal bovine serum (FBS) and 10% dimethylsulfoxyde (DMSO) for gradual cooling in a CoolCell chamber.

Single cell preparation for pig model

Blood samples were processed as described previously (see Methods 1.2). After filtering, cells were centrifugated at 300g for 10 minutes at 4°C and resuspended in staining buffer for the HTO antibody labeling (see Methods 1.3). The sequenced libraries were aligned to the Sscrofa 11.1 (February 2017 release) reference genome with CellRanger v5.0.0.

Pig biopsy immunostaining analysis

Kidney biopsies fixed Carnoy's solution for 30 minutes followed by a fixation in formaldehyde for 24h for optical microscopy purpose. A second batch of kidney biopsies was prepared for immunostaining purpose: biopsies were placed in cryomold, covered with optimal cutting temperature (OCT) compound and immersed in cold isopentane. Following their solidification, cryomolds were stored in liquid nitrogen. Cryosectioning was performed and the resulting slides of kidney biopsies were stained with periodic acid-Schiff (PAS) and Masson's trichrome stains (TM).

The cellular infiltration was counted using ImageJ[52] software on the PAS-stained kidney biopsies. Areas of interest were selected to exclude areas with glomeruli. Pictures were first converted to 8-bit grayscale, and the threshold of detection was set to capture only the stained cells.

3. ALARM analysis in distinct disease conditions

Analysis of the ALARM module in kidney biopsies

Two separate studies were analyzed here. The Reeve *et al.* Affymetrix Microarray data in RAW CEL format was downloaded from Gene Expression Omnibus (GEO) website with accession number GSE98320. The samples were pre-processed using robust multi-chip averaging (RMA) implemented in Bioconductor. The patient condition was obtained from the 'd96' metadata column as designated in the corresponding Series Matrix file. The patients strictly defined as either TCMR (n=76), ABMR (n=197), Mixed (n=39) or no major abnormality (STA, n=257) as a stable condition, were retained for downstream analysis. The Callemeyn *et al.* dataset was downloaded from GEO with accession number GSE147089. The CEL files were similarly pre-processed using the RMA method. The labels for each sample were obtained from the Series Matrix file and the phenotypes are defined as biopsies without ABMR (n=168), DSA negative ABMR (n=26) and DSA positive ABMR (n=30).

The score used to stratify patients was computed by averaging the z-scores of the ALARM module genes.

ALARM mean z-score distribution across conditions

The Kolmogorov-Smirnov (KS) test was then used to compare the distribution of the ALARM module score between stable and rejection conditions. This non-parametric statistical test compares the cumulative distribution functions of the mean ALARM z-scores in both groups. The KS test statistic (D) is the maximum vertical distance between the two distributions. The p-value of the test is the

probability of obtaining a test statistic as extreme as D or more extreme, assuming that the null hypothesis is true. The null hypothesis is that the two samples are drawn from the same distribution.

Receptor-Ligand analysis

The 'iTalk' R package was used for the receptor-ligand (RL) analysis. The receptors were gene candidates in single-cell kidney transplant stable and rejection patients. The *rawParse()* function with `stats='mean'` was used to identify the candidate genes. For each celltype, the genes were ordered by their average count expression. Only the top 50 percent of these genes were selected for the subsequent RL analysis. The same criteria were adopted for selecting the ligand candidates from the bulk RNAseq biopsy data. The significant interaction pairs were discovered from the iTalk database restricted on the cytokine interactions only.

Analysis of publicly available scRNA-seq datasets

PBMCs of 45 healthy Volunteers (Van Der Wijst MG et al.):

Processed (de-anonymized) single-cell RNA-seq data and its relevant meta data was obtained from the European Genome-phenome Archive (EGA) accession number EGAS00001002560. The available data was merged to build a single Seurat object for downstream analysis. Azimuth reference for PBMCs was used to annotate the cells.

LPS and Covid PBMC dataset (Stephenson et al.):

The processed data was downloaded from Array Express under accession number E-MTAB-10026. Only individuals from the same batch containing the LPS-treated volunteers were selected to mitigate batch effects. Fig 5B shows only those individuals where the major cell types were available. The Covid patients originally annotated as Mild/Moderate was included as 'Moderate' in Fig 5D.

Sepsis-PBMC Dataset (Reyes et al.):

The pre-processed scRNA-seq data was downloaded through the Broad Institute Single Cell Portal (SCP548). The data was further analyzed with Seurat to obtain the Module score based on UCell.

Covid – BALF Dataset (Liao et al.):

The data was accessed from GSE145926. The filtered cell matrix was processed with Seurat with the code as provided by the authors of the original article.

Analysis of publicly available data set of 10 immune mediated diseases (Ota et al.)

Bulk RNAseq of 28 pure immune cell types from 339 individuals divided into 10 immune-mediated diseases and 92 healthy controls was obtained from the National Bioscience Database Center (NBDC) Human Database with the accession number E-GEAD-397. The dataset was assembled as a large matrix with genes listed in rows and columns are individuals with homogeneous cell types. Functions from the Seurat pipeline were used to compute the module scores and generate the population's UMAP embedding.

Disease Classification

Combined diseases vs healthy approach was deployed for each major cell type and by cell subtype at the primary level. The Logistic Regression classifier from the R package 'caret' and the repeated cross-validation strategy for model evaluation were used.

In the next phase, for each major cell type, classification was evaluated for Healthy vs One Disease. An identical classification model was built in this phase as well. The coefficient of variation (CV^2)[53] method produced an unsupervised set of highly variable genes as a control for the ALARM module genes. The mean vs (variance/$means^2$) was modelled with *glmgam.fit* from the *statmod* R package

for the variance estimate of every gene. The genes were ranked by the significance of deviation from the fit. The same number of variable genes was then used in the modules.

Gene association to disease terms

The association between the ALARM genes and immune disease terms was performed using the disgenet2r (v0.99.2) R package [43]. The ratio of genes associated with immune diseases to the total number of genes within the modules was compared to the corresponding ratio obtained from 1000 randomly selected sets of 61 genes.

Acknowledgements:

We are most grateful to the Genomics Core Facility **GenoA**, member of Biogenouest and France Genomique and to the Bioinformatics Core Facility **BiRD**, member of Biogenouest and Institut Français de Bioinformatique (IFB) (ANR-11-INBS-0013) for the use of their resources and their technical support. DS was supported by Progreffe foundation. The project was supported by Region Pays de Loire "Etoile Montantes" grant for JP. We would like to thank the members of the DIVAT consortium for their involvement in the study, the physicians who helped recruit patients, and all patients who participated in this study. We also thank the clinical research associates who participated in the data collection. Data were collected from the French DIVAT multicentric prospective cohort of kidney and/or pancreatic transplant recipients (www.divat.fr, N° CNIL 914184, ClinicalTrials.gov recording: NCT02900040). We also thank the biological resource centre for biobanking (CHU Nantes, Nantes Université, Centre de ressources biologiques (BB-0033-00040), F-44000 Nantes, France). The authors have no conflicting financial interests.

Contributions:

TL, DS & JP analyzed the data and wrote the manuscript. CF and TL performed scRNA-seq experiments. TL and SV, JB and GB performed pig transplantation model experiments. LBD performed cell sorting experiments. CK, RD, MG and SB collected and provided patient data and kidney transplantation PBMC samples. ND, AR, RJ, SB contributed to study design, result interpretation and critically revised the manuscript. All authors contributed to the draft of the manuscript. JP conceived the study and oversaw all experiments and analyses in this study.

Data availability

The data underlying Figures 1,2 and 3 will be openly available in ENA once the article has been peer-reviewed.

Figure legends:

Fig 1. Comprehensive longitudinal single-cell RNA-sequencing of circulating immune cells in a cohort of kidney allograft recipient.

A) Timeline of the blood sampling points post-transplantation for the patients followed longitudinally. STA=Stable patient (n=3), TCMR=T cell mediated rejection (n=3), ABMR=Antibody-mediated rejection (n=3). Tolerant patients are not shown.

B) Schematic diagram of the scRNA-seq preparation workflow using cell hashing. Peripheral blood mononuclear cells (PBMCs) were collected from stable, ABMR and TCMR patients and then stained with one different oligo-conjugated antibody before being pooled and processed using microfluidic encapsulation.

C) UMAP dimensional-reduction embedding of the integrated samples (n=30). Each colour represents a different cell subpopulation, adapted and manually curated from the automatic Azimuth annotation.

D) UMAP projection showing the disease state distribution, TOL=Tolerant patients.
E) UMAP projection coloured according to experimental batch of origin

Fig 2. ALARM Module identification
A) Schematic workflow of the gene co-expression analysis using consensus nonnegative matrix factorisation (cNMF) module detection separate in each batch. The module selection was then refined based on overlapping genes between the three batches.
B) Clustering of 9 modules across the 3 batches, using the Jaccard distance.
C) Heatmap showing the combined gene expression of each module, i.e. module scores of the 9 modules summarized for each distinct cell-type.
D) UMAP projection of the expression of Module 9 across all cells.
E) Regression analysis of the 9 modules by cell types. The outcome variable (y) was time (T0, T1 and T2) and the independent variable (x) was the module score. Heatmap shows the beta values (trend) for each cell-type and disease state. Negative values correspond to a decrease of the module score across the three time points, positive values to an increase.
F) Super violin plots[54] showing the longitudinal trend of ALARM module in NK, CD4 T cells (top), CD8 T cells and B cells (bottom), stratified by individuals from each batch.
G) Gene Ontology analysis of biological process (BP) and molecular function (MF) identified by comparing the ALARM gene enrichment using the 4000 most variable genes as background (See Supplemental file 1).

Fig 3. Pig model scRNA-seq analysis
A) Schematic diagram of the acute kidney allograft rejection in pig model. Recipient pig with a unilateral nephrectomy received a kidney graft from a second healthy pig. Kidney biopsies and PBMCs were collected daily and observed in immunohistochemistry. PBMCs were prepared for a scRNA-seq analysis.
B) Immunohistochemistry of pig biopsies stained with Periodic Aid Schiff (PAS), to stain polysaccharides, glycoproteins and glycolipids at day 0, day 2, day 4 and day 6
C) Quantification of cell populations in the kidney graft at given days using Image J cell counting software (See supplemental figure 3 for details)
D) UMAP dimensional-reduction projection of the circulating immune cell types (PBMCs) scRNA-seq after PBMC isolation at D0, D2, D4 and D6.
E) Proportions of circulating immune cells (PBMC) across the different time points (D0-D6) in the recipient transplanted pig.
F) Violin plot of the ALARM module score in B cells, monocytes, CD4 T cells, CD8 T cells and NK cells throughout acute rejection in the kidney tissues (Day 0, Day2, Day 4 Day6). *$P < 0.05$, **$P < 0.01$, ***$P < 0.001$, ****$P < 0.0001$.

Fig 4. ALARM gene expression increases in kidney tissues during rejection
Left panels from Reeve et al., 2017 and right panels from Callemeyn et al 2020. STA =Stable patient, ABMR=Antibody-mediated rejection, TCMR=T cell mediated rejection, Mixed=Graft undergoing ABMR and TCMR, DSA- = Donor specific antibody negative and DSA+= Donor specific antibodies positive.
A) Violin plot of the sum of z-scores of ALARM genes across conditions. Wilcoxon P-values are shown in panel comparing Stable (STA) to rejection status (ABMR, Mixed or TCMR and DSA- and DSA+ ABMR). The mean comparison p-values were computed using the Wilcoxon rank-sum test.B) Heatmap showing z-scores of ALARM genes (one gene per row) in all graft biopsies. Phenotype denotes the disease states. Patients are sorted on the mean of the module gene z-scores.
C) Cumulative distribution of the mean of z-scores of ALARM genes comparing stable vs the combined rejection conditions. K-S = Kolmogorov -Smirnov P-values and distance.

D) Ligand-Receptor analysis between receptors genes identified in circulating immune cells and cytokines genes expressed in the allograft kidney tissue under no rejection and rejection condition. Width of the arrow line is proportional to the expression of the ligands and the width of the arrowhead is proportional to the receptor. Only the top 5 associations from each cell type of differentially expressed receptors (PBMC scRNA-seq) and cytokines (Biopsy microarray) are shown.
E) Boxplots showing CXCL12 expression in biopsies from patients with high ALARM module expression (>75%), medium (25-75%) and low (<25%). Wilcoxon rank-sum test was used to calculate P-values shown above.

Fig 5. ALARM gene expression is altered in distinct immune-conditions
A) ALARM module score distribution by cell type based on scRNA-seq analysis of PBMC from 45 unrelated healthy individuals (Wijst et al.)
B) Outline of study on Lipopolysaccharide (LPS) intravenous injection (i.v.) scRNAseq experiment performed on healthy volunteers obtained from Stephenson et al. The annotated expression data was used to compute the ALARM module score across time points after LPS injection in healthy volunteers. Violin plots show the module score across cell types and condition. Total number of cells are mentioned below the plot. P-values are shown above the violin plots and were calculated using Wilcoxon rank sum test comparing each cell type between healthy and LPS conditions.
C) Violin plots of ALARM module score for three individuals which had matching timepoints across all cell types in the condition LPS 90 min and LPS 10h. Lines connect the median ALARM module score across time points for each individual separately. P-values are shown above the violin plots and were calculated using Wilcoxon rank sum test comparing the two distinct time points.
D) Outline of patients with sepsis and urinary tract infection obtained from Reyes et al,. Annotated data was used to compute ALARM module score across the different cell-types in urinary tract infection (UTI) patients and bacteraemia sepsis patients. Number of cells and individuals used are shown below the violin plots. P-values are shown above the violin plots and were calculated using Wilcoxon rank sum test comparing each cell type between healthy and LPS conditions.
E) Outline of PBMC scRNA-seq generated on healthy individuals, moderate covid-19 and severe covid-19 patients (Stephenson et al.,) and Bronchoalveolar lavage fluid (BALF) from a distinct cohort (Liao et al.). Upper panel shows median ALARM module score for each cell-type for PBMC (blue) and BALF (red). Lower panel shows for each cell-type the module score for each corresponding cell-type specific module.

Figure 6 ALARM genes are implicated in and predictive of immune mediated diseases
A) UMAP of bulk transcriptomic study (Ota et al., 2020). Colours represent major cell types and each single point represents a bulk transcriptomic dataset. Cell sub types are annotated in the plot.
B) The same UMAP showing expression of ALARM module expression across samples.
C) Outline of classification approach used to test disease prediction
D) Barchart showing the F-1 score of disease classification for ALARM, cell-type specific modules and coefficient of variation (CV^2) selected genes in each major cell type separately.
E) Barchart of F1-scores computed for disease classification in each sub cell type separately for ALARM and CV^2 genes
F) Radar chart showing the F1-score in each cell type for classification between each disease and healthy separately using ALARM genes in each major cell type.
G) Barchart showing the top three enriched diseases in the ALARM genes using the DisGeNET curated database.

Fig 1S. ScRNA-seq integration of a cohort of kidney allograft recipients
A) Expression profiles of cell-specific markers distinguish the PBMC populations. Average expression is the log-normalized expression average of the cells by cell type, size of the dots is associated to the fraction of cells of the cluster in which the gene is detected.

B) Cell type proportion by cluster in the overall PBMC population. Comparison include Stable patients, Rejection (ABMR+TCMR) and two public datasets: healthy volunteers from Stephenson et al, 2021, and healthy volunteers from Reyes et al, 2020. One-way ANOVA with Tukey's multiple comparisons post hoc test was performed, *P < 0.05, **P < 0.01, ***P < 0.001, ****P < 0.0001.
C) UMAP projection showing the sample distribution, ABMR=Humoral rejection, TCMR=Cellular rejection, STA=Stable, TOL=Tolerant. Second UMAP shows the timepoint distribution, T0=Time point 0 (Graft), T1=Time point 1, T2=Time point 2.
D) K-bet acceptance rate by cell types following the MNN batch integration. Complete k-bet acceptance rate was computed on the overall PBMC population.

Fig 2S. Assessing module distribution
A) Alluvial plot showing the shared origin of each module across batches. Each cell is assigned to the most enriched module they express.
B) Boxplots showing the distribution of Pearson correlation coefficient *R* of pairwise gene expression correlation by cell type across modules. A module of random genes was generated to compare with the nine other modules. Multiple gene pairs from each module are selected to compute the rho values using a subset of common cells within the cell type. 1000 repetitions of 50 pairs each yielded 50000 *R* values, as represented in every box. The subset of common cells changes with every repetition.
C) Boxplots showing the distribution of Pearson correlation coefficient *R* of pairwise gene expression correlation by cell type for Module 9.

Fig 3S. Cellular characterization of pig PBMC by scRNA-seq analysis
A) Image J analysis of immuno-stained slices to quantify cell infiltration. Red boxes show counting areas which excludes glomeruli. Right panel shows the cells which were then counted using Image J software.
B) Pig data were annotated using the Sscrofa reference genome and associated to their human homologue. The expression profiles of cell type-specific markers is shown in the dotplot of relative expression by cell type. Size of the dots are associated to the fraction of cells of the cluster in which the gene is detected. The UMAP embeds the 4 samples (D0, D2, D4, D6) with their corresponding cell type annotation.

Fig 5S. Overview of the cohort distribution
A) ALARM module score distribution across sex. No significance was found for the sex parameter with a t-test.
B) ALARM module score distribution across age categories. No significance was found for the age parameter with a one-way ANOVA test.

Fig 6S. ALARM genes can classify immune-mediated diseases
A) Distribution of the bulk RNA-seq samples across the 28 circulating immune cell types for the 337 patients distributed across 10 immune mediated diseases and the 79 healthy controls.
B) Area Under Curve (AUC) and Cohen's Kappa score across cell types in disease and healthy patients.
C) AUC and Cohen's Kappa score across cell subtypes in disease and healthy patients
D) Distribution of the ratio of genes associated to Gene-Disease Association (GDA) terms in 1000 modules of 61 randomly selected genes. The ALARM module has a ratio of 0.39 genes associated to GDA terms (red line).

References:

1. Reyes, M. *et al.* An immune cell signature of bacterial sepsis. *Nat. Med.* **26**, 333–340 (2020).

2. Perez, R. K. *et al.* Single-cell RNA-seq reveals cell type-specific molecular and genetic associations to lupus. *Science* **376**, eabf1970 (2022).
3. Kazer, S. W. *et al.* Integrated single-cell analysis of multicellular immune dynamics during hyperacute HIV-1 infection. *Nat. Med.* **26**, 511–518 (2020).
4. Zhang, F. *et al.* Defining inflammatory cell states in rheumatoid arthritis joint synovial tissues by integrating single-cell transcriptomics and mass cytometry. *Nat. Immunol.* **20**, 928–942 (2019).
5. Stephenson, E. *et al.* Single-cell multi-omics analysis of the immune response in COVID-19. *Nat. Med.* **27**, 904–916 (2021).
6. Bernardes, J. P. *et al.* Longitudinal Multi-omics Analyses Identify Responses of Megakaryocytes, Erythroid Cells, and Plasmablasts as Hallmarks of Severe COVID-19. *Immunity* **53**, 1296-1314.e9 (2020).
7. Chaumette, T. *et al.* Monocyte Signature Associated with Herpes Simplex Virus Reactivation and Neurological Recovery After Brain Injury. *Am. J. Respir. Crit. Care Med.* (2022) doi:10.1164/rccm.202110-2324OC.
8. del Rosario, R. C. H. *et al.* Histone acetylome-wide associations in immune cells from individuals with active Mycobacterium tuberculosis infection. *Nat. Microbiol.* **7**, 312–326 (2022).
9. Kotliar, D. *et al.* Identifying gene expression programs of cell-type identity and cellular activity with single-cell RNA-Seq. *eLife* **8**, e43803 (2019).
10. Loupy, A., Mengel, M. & Haas, M. Thirty years of the International Banff Classification for Allograft Pathology: the past, present, and future of kidney transplant diagnostics. *Kidney Int.* **101**, 678–691 (2022).
11. Sirota, M. & Sarwal, M. M. Transplantomics: Toward Precision Medicine in Transplantation Research. *Transplantation* **101**, 1777–1782 (2017).
12. Moreau, A., Varey, E., Anegon, I. & Cuturi, M.-C. Effector Mechanisms of Rejection. *Cold Spring Harb. Perspect. Med.* **3**, a015461 (2013).

13. Stoeckius, M. *et al.* Cell Hashing with barcoded antibodies enables multiplexing and doublet detection for single cell genomics. *Genome Biol.* **19**, 224 (2018).

14. Stuart, T. *et al.* Comprehensive integration of single-cell data. *Cell* **177**, 1888-1902.e21 (2019).

15. Hao, Y. *et al.* Integrated analysis of multimodal single-cell data. *Cell* **184**, 3573-3587.e29 (2021).

16. Büttner, M., Miao, Z., Wolf, F. A., Teichmann, S. A. & Theis, F. J. A test metric for assessing single-cell RNA-seq batch correction. *Nat. Methods* **16**, 43–49 (2019).

17. Langfelder, P. & Horvath, S. WGCNA: an R package for weighted correlation network analysis. *BMC Bioinformatics* **9**, 559 (2008).

18. Nestorowa, S. *et al.* A single-cell resolution map of mouse hematopoietic stem and progenitor cell differentiation. *Blood* **128**, e20–e31 (2016).

19. Yamashita, I., Nagata, T., Tada, T. & Nakayama, T. CD69 cell surface expression identifies developing thymocytes which audition for T cell antigen receptor-mediated positive selection. *Int. Immunol.* **5**, 1139–1150 (1993).

20. Ziegler, S. F., Ramsdell, F. & Alderson, M. R. The activation antigen CD69. *Stem Cells* **12**, 456–465 (1994).

21. Werfel, T., Boeker, M. & Kapp, A. Rapid expression of the CD69 antigen on T cells and natural killer cells upon antigenic stimulation of peripheral blood mononuclear cell suspensions. *Allergy* **52**, 465–469 (1997).

22. Turner, J.-E., Becker, M., Mittrücker, H.-W. & Panzer, U. Tissue-Resident Lymphocytes in the Kidney. *J. Am. Soc. Nephrol. JASN* **29**, 389–399 (2018).

23. López-Cabrera, M. *et al.* Transcriptional Regulation of the Gene Encoding the Human C-type Lectin Leukocyte Receptor AIM/CD69 and Functional Characterization of Its Tumor Necrosis Factor-α-responsive Elements (∗). *J. Biol. Chem.* **270**, 21545–21551 (1995).

24. Castellanos, M. C. *et al.* Expression of the leukocyte early activation antigen CD69 is regulated by the transcription factor AP-1. *J. Immunol. Baltim. Md 1950* **159**, 5463–5473 (1997).

25. Tögel, F., Isaac, J., Hu, Z., Weiss, K. & Westenfelder, C. Renal SDF-1 signals mobilization and homing of CXCR4-positive cells to the kidney after ischemic injury. *Kidney Int.* **67**, 1772–1784 (2005).

26. Song, A., Jiang, A., Xiong, W. & Zhang, C. The Role of CXCL12 in Kidney Diseases: A Friend or Foe? *Kidney Dis.* **7**, 167–176 (2021).

27. Hoffmann, U. *et al.* SDF-1 expression is elevated in chronic human renal allograft rejection. *Clin. Transplant.* **20**, 712–718 (2006).

28. Pabst, R. The pig as a model for immunology research. *Cell Tissue Res.* **380**, 287–304 (2020).

29. Reeve, J. *et al.* Assessing rejection-related disease in kidney transplant biopsies based on archetypal analysis of molecular phenotypes. *JCI Insight* **2**, 94197 (2017).

30. Callemeyn, J. *et al.* Transcriptional Changes in Kidney Allografts with Histology of Antibody-Mediated Rejection without Anti-HLA Donor-Specific Antibodies. *J. Am. Soc. Nephrol.* **31**, 2168–2183 (2020).

31. Moll, N. M. & Ransohoff, R. M. CXCL12 and CXCR4 in bone marrow physiology. *Expert Rev. Hematol.* **3**, 315–322 (2010).

32. Yellowley, C. CXCL12/CXCR4 signaling and other recruitment and homing pathways in fracture repair. *BoneKEy Rep.* **2**, 300 (2013).

33. Burger, J. A. & Kipps, T. J. CXCR4: a key receptor in the crosstalk between tumor cells and their microenvironment. *Blood* **107**, 1761–1767 (2006).

34. van der Wijst, M. G. P. *et al.* Single-cell RNA sequencing identifies celltype-specific cis-eQTLs and co-expression QTLs. *Nat. Genet.* **50**, 493–497 (2018).

35. Tigchelaar, E. F. *et al.* Cohort profile: LifeLines DEEP, a prospective, general population cohort study in the northern Netherlands: study design and baseline characteristics. *BMJ Open* **5**, e006772 (2015).

36. Vos, A. F. de *et al.* In Vivo Lipopolysaccharide Exposure of Human Blood Leukocytes Induces Cross-Tolerance to Multiple TLR Ligands. *J. Immunol.* **183**, 533–542 (2009).

37. Andonegui, G., Goyert, S. M. & Kubes, P. Lipopolysaccharide-Induced Leukocyte-Endothelial Cell Interactions: A Role for CD14 Versus Toll-Like Receptor 4 Within Microvessels1. *J. Immunol.* **169**, 2111–2119 (2002).

38. Beutler, B. TLR4 as the mammalian endotoxin sensor. *Curr. Top. Microbiol. Immunol.* **270**, 109–120 (2002).

39. Beutler, B., Du, X. & Poltorak, A. Identification of Toll-like receptor 4 (Tlr4) as the sole conduit for LPS signal transduction: genetic and evolutionary studies. *J. Endotoxin Res.* **7**, 277–280 (2001).

40. Liao, M. *et al.* Single-cell landscape of bronchoalveolar immune cells in patients with COVID-19. *Nat. Med.* **26**, 842–844 (2020).

41. Mi, Z., Guo, B., Yin, Z., Li, J. & Zheng, Z. Disease classification via gene network integrating modules and pathways. *R. Soc. Open Sci.* **6**, 190214 (2019).

42. Ota, M. *et al.* Dynamic landscape of immune cell-specific gene regulation in immune-mediated diseases. *Cell* **184**, 3006-3021.e17 (2021).

43. Piñero, J. *et al.* The DisGeNET knowledge platform for disease genomics: 2019 update. *Nucleic Acids Res.* **48**, D845–D855 (2020).

44. Cibrián, D. & Sánchez-Madrid, F. CD69: from activation marker to metabolic gatekeeper. *Eur. J. Immunol.* **47**, 946–953 (2017).

45. Afeltra, A. *et al.* Expression of CD69 antigen on synovial fluid T cells in patients with rheumatoid arthritis and other chronic synovitis. *Ann. Rheum. Dis.* **52**, 457–460 (1993).

46. Su, C. C., Shau, W. Y., Wang, C. R., Chuang, C. Y. & Chen, C. Y. CD69 to CD3 ratio of peripheral blood mononuclear cells as a marker to monitor systemic lupus erythematosus disease activity. *Lupus* **6**, 449–454 (1997).

47. Britton, C., Poznansky, M. C. & Reeves, P. Polyfunctionality of the CXCR4/CXCL12 axis in health and disease: Implications for therapeutic interventions in cancer and immune-mediated diseases. *FASEB J. Off. Publ. Fed. Am. Soc. Exp. Biol.* **35**, e21260 (2021).

48. Abidi, A. *et al.* Characterization of Rat ILCs Reveals ILC2 as the Dominant Intestinal Subset. *Front. Immunol.* **11**, (2020).

49. Drouin, M. *et al.* CLEC-1 is a death sensor that limits antigen cross-presentation by dendritic cells and represents a target for cancer immunotherapy. *Sci. Adv.* **8**, eabo7621 (2022).

50. Feregrino, C. & Tschopp, P. Assessing evolutionary and developmental transcriptome dynamics in homologous cell types. *Dev. Dyn.* **251**, 1472–1489 (2022).

51. Andreatta, M. & Carmona, S. J. UCell: Robust and scalable single-cell gene signature scoring. *Comput. Struct. Biotechnol. J.* **19**, 3796–3798 (2021).

52. Schneider, C. A., Rasband, W. S. & Eliceiri, K. W. NIH Image to ImageJ: 25 years of image analysis. *Nat. Methods* **9**, 671–675 (2012).

53. Brennecke, P. *et al.* Accounting for technical noise in single-cell RNA-seq experiments. *Nat. Methods* **10**, 1093–1095 (2013).

54. Kenny, M. & Schoen, I. Violin SuperPlots: visualizing replicate heterogeneity in large data sets. *Mol. Biol. Cell* **32**, 1333–1334 (2021).

Figure 1

A

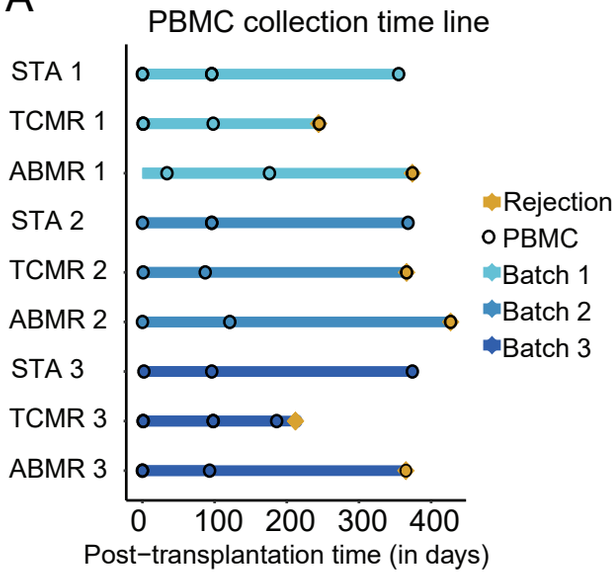

B

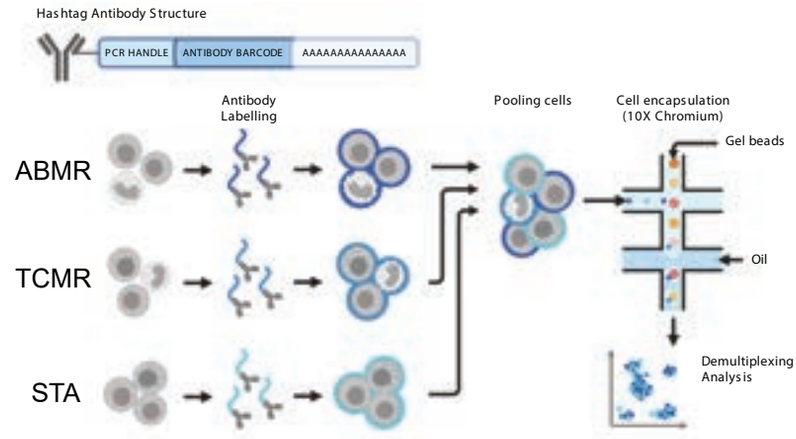

C

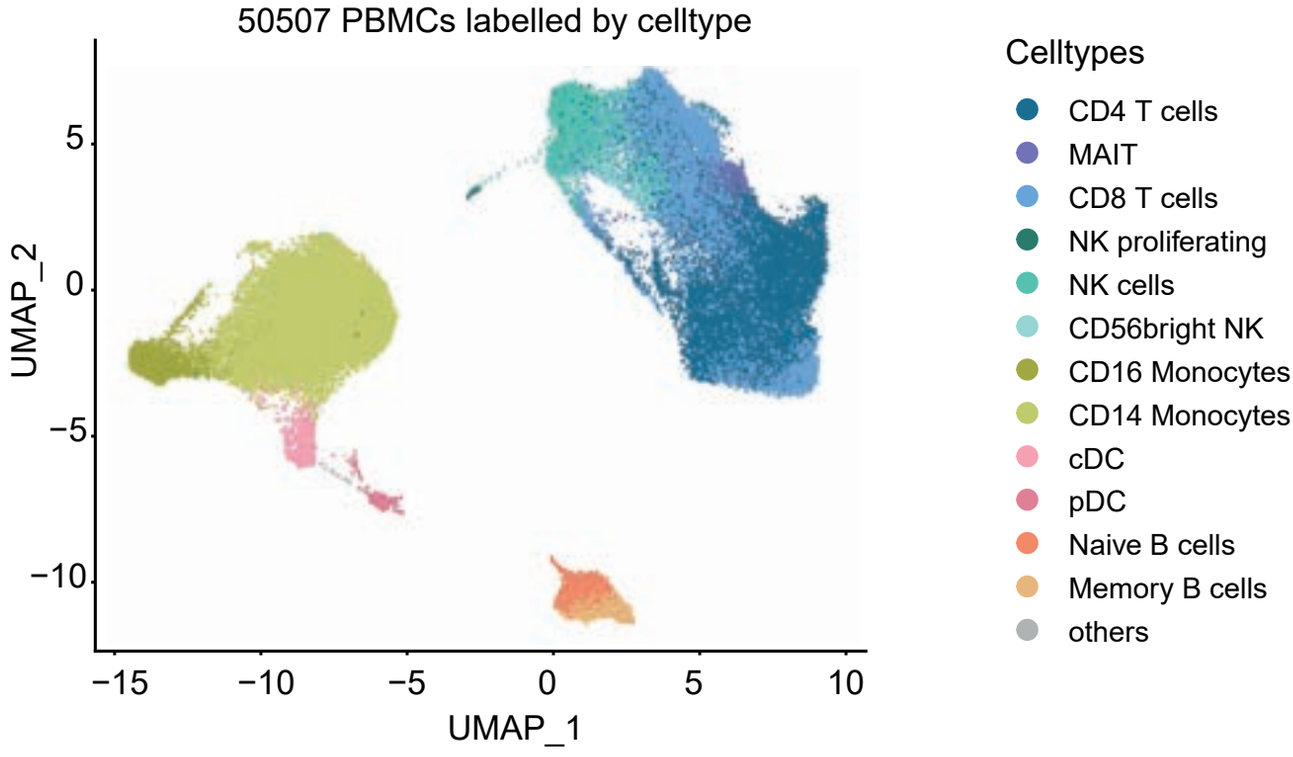

D

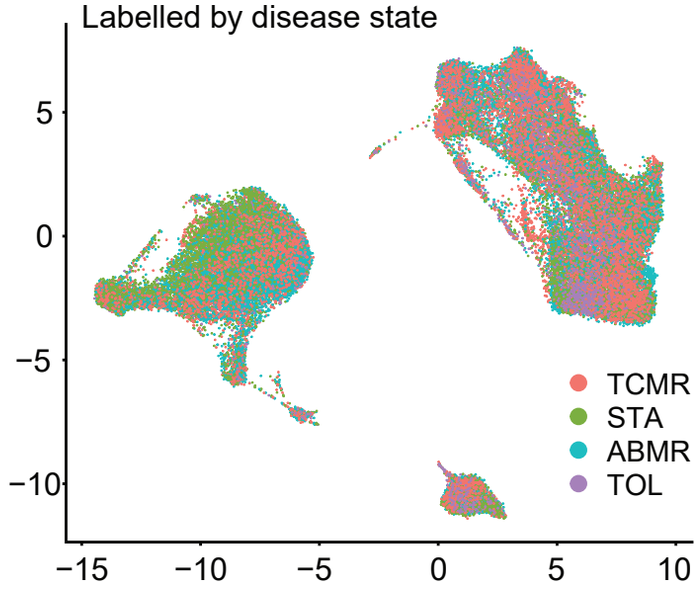

E

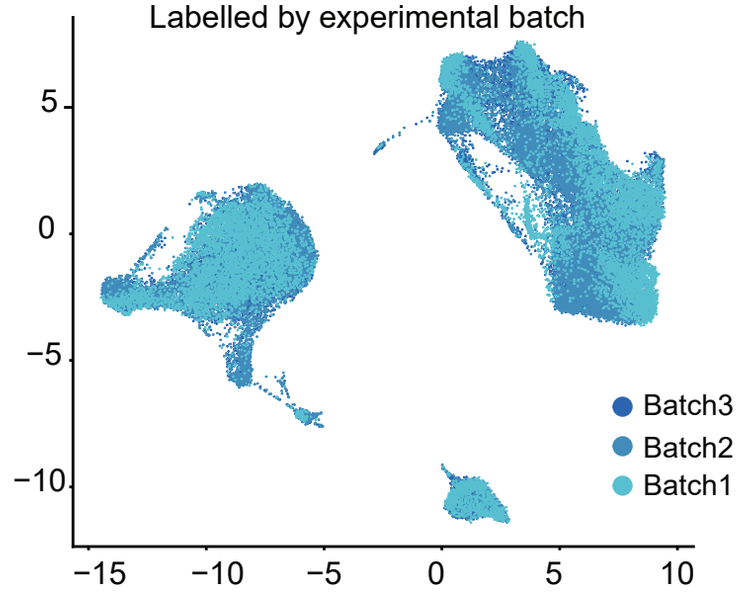

Supp. Figure 1

A

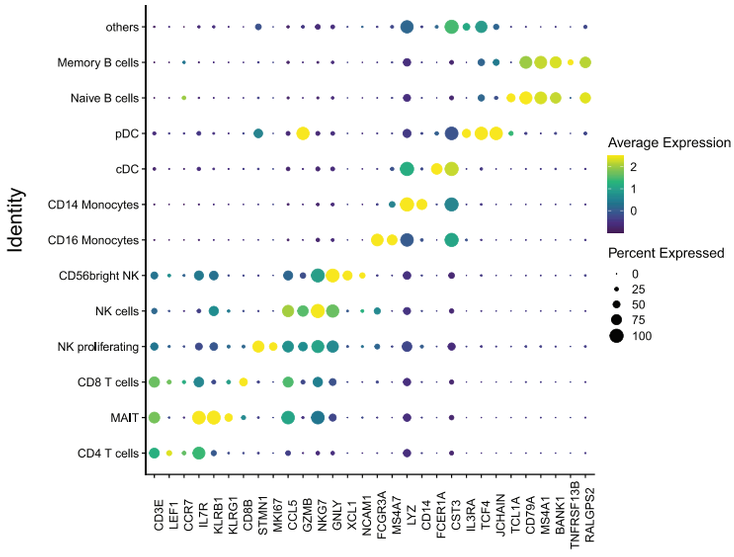

B

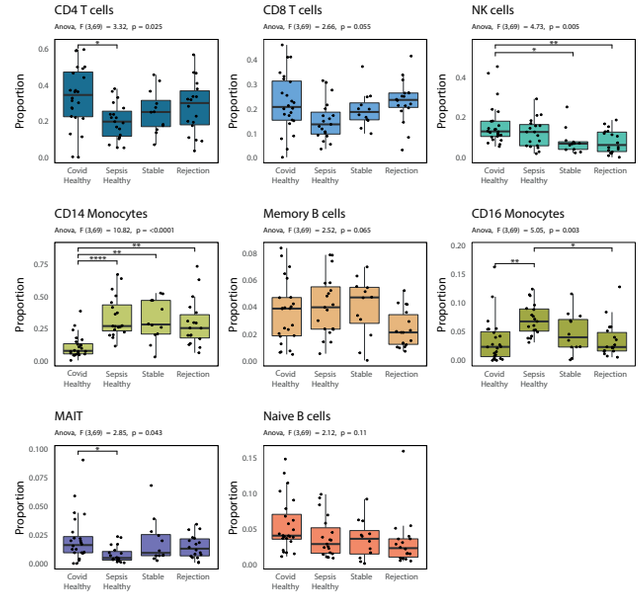

C

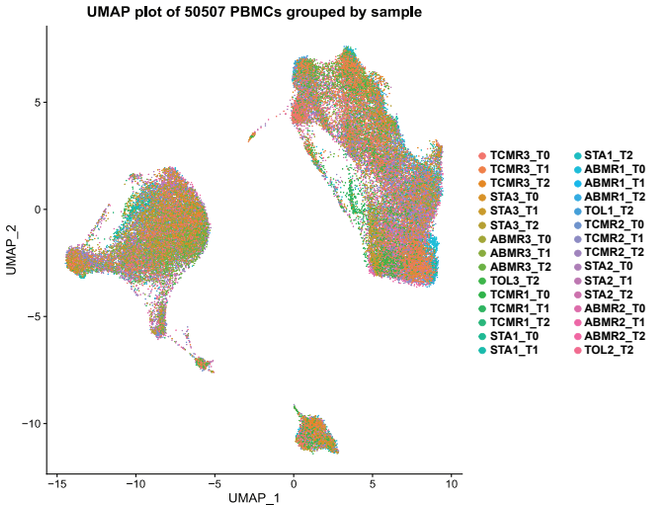

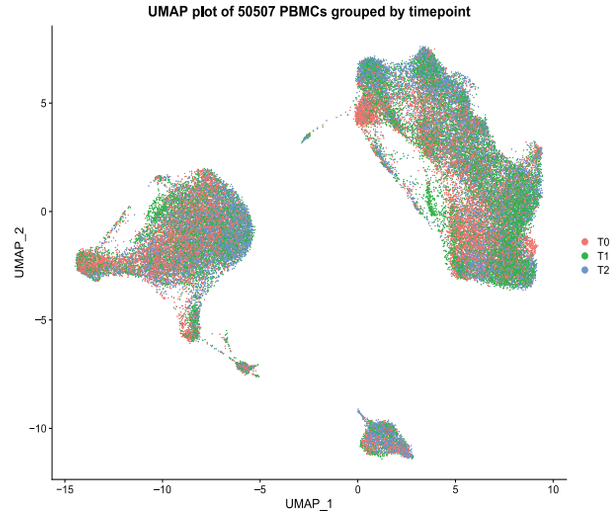

D

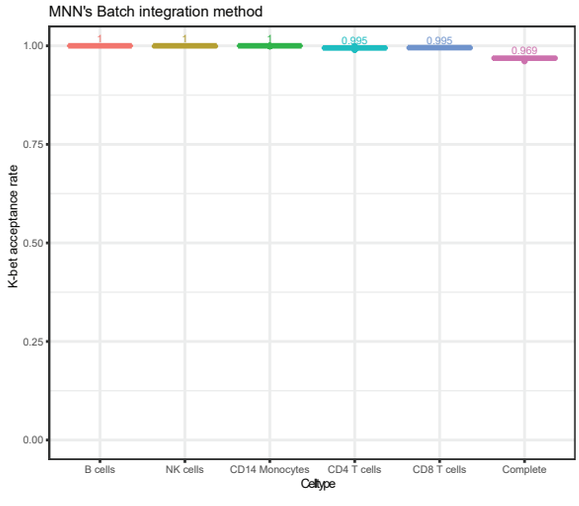

Figure 2

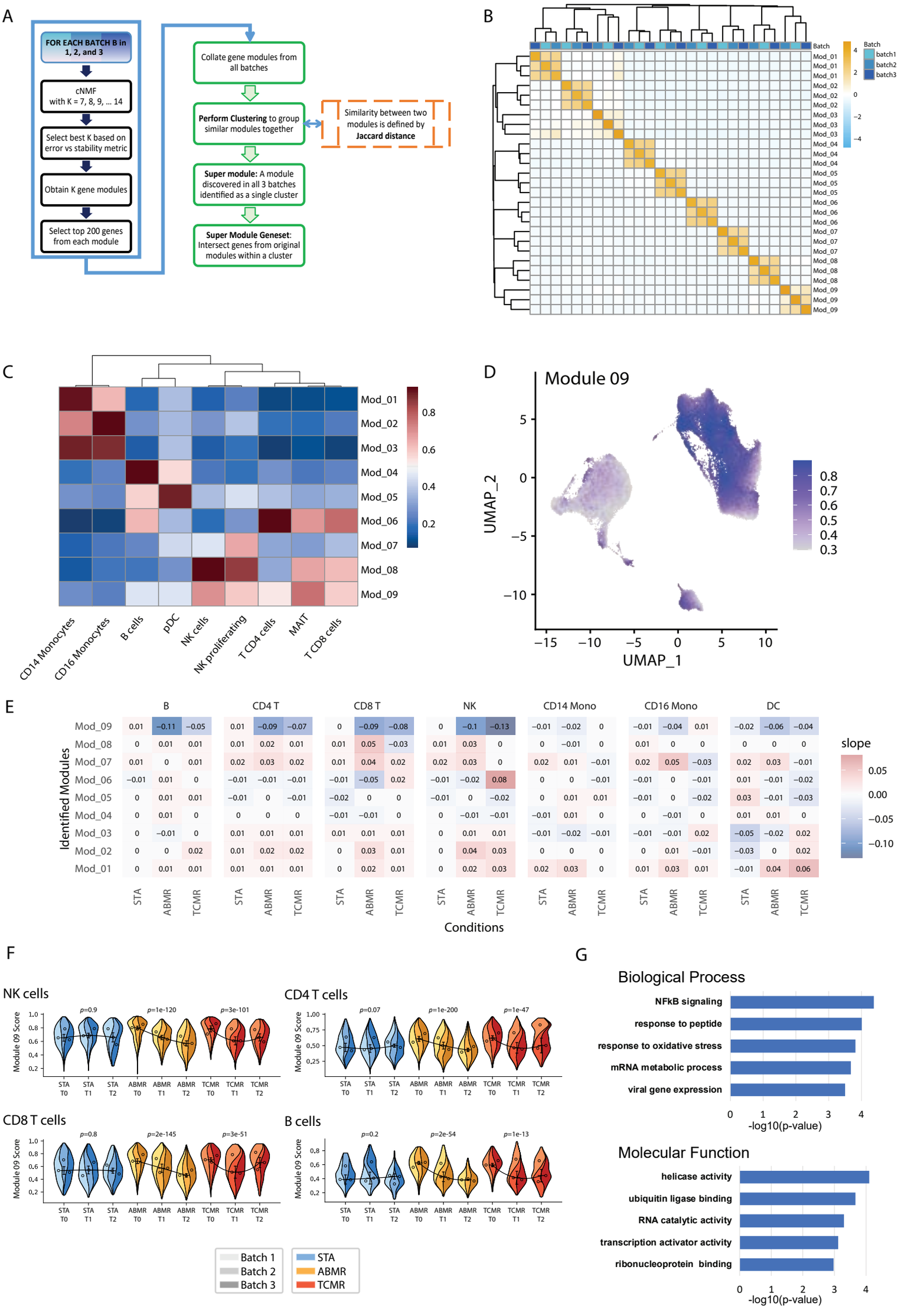
A
FOR EACH BATCH B in 1, 2, and 3
cNMF with K = 7, 8, 9, ... 14
Select best K based on error vs stability metric
Obtain K gene modules
Select top 200 genes from each module
Collate gene modules from all batches
Perform Clustering to group similar modules together
Similarity between two modules is defined by Jaccard distance
Super module: A module discovered in all 3 batches identified as a single cluster
Super Module Geneset: Intersect genes from original modules within a cluster
B
Batch
batch1
batch2
batch3
C
CD14 Monocytes
CD16 Monocytes
B cells
pDC
NK cells
NK proliferating
T CD4 cells
MAIT
T CD8 cells
D
Module 09
UMAP_2
UMAP_1
E
Identified Modules
Conditions
slope
F
NK cells
CD4 T cells
CD8 T cells
B cells
Module 09 Score
Batch 1
Batch 2
Batch 3
STA
ABMR
TCMR
G
Biological Process
NFkB signaling
response to peptide
response to oxidative stress
mRNA metabolic process
viral gene expression
-log10(p-value)
Molecular Function
helicase activity
ubiquitin ligase binding
RNA catalytic activity
transcription activator activity
ribonucleoprotein binding
-log10(p-value)

Supp. Figure 2

A

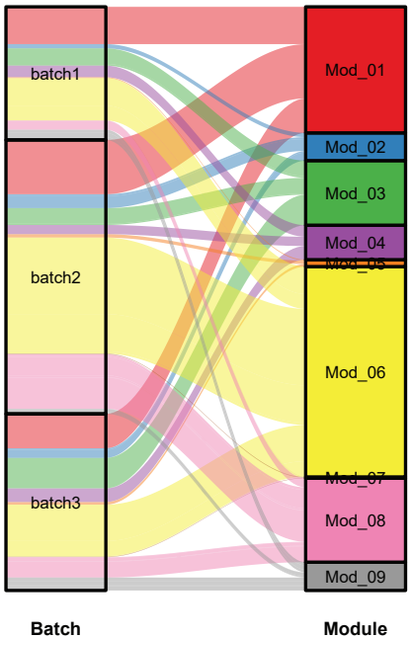

B

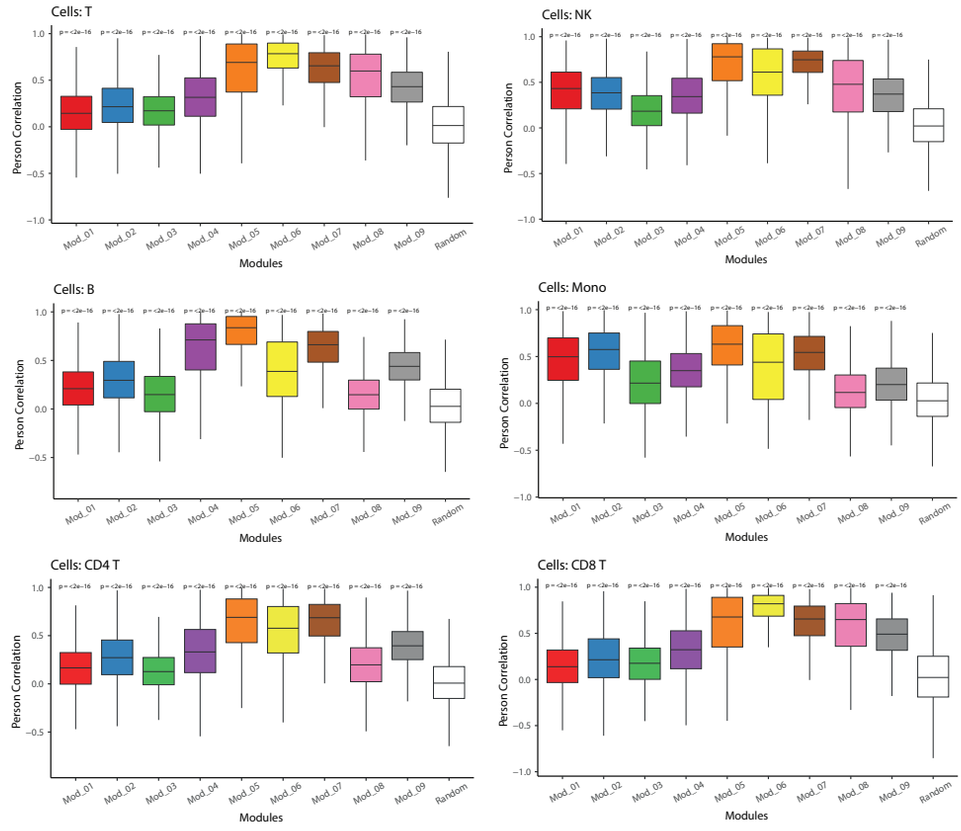

C

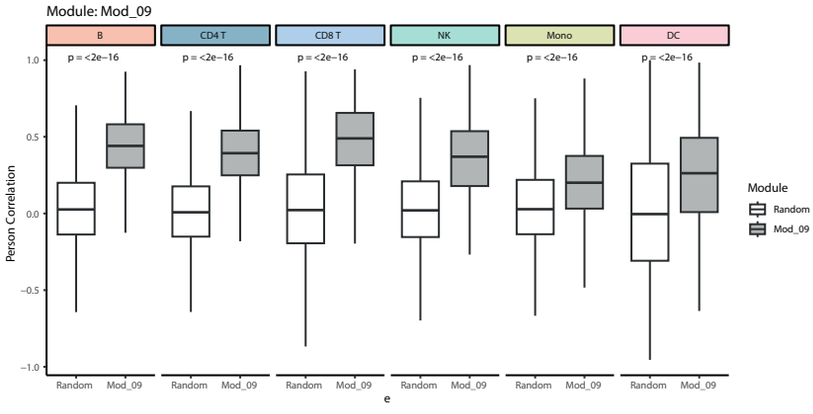

Figure 3

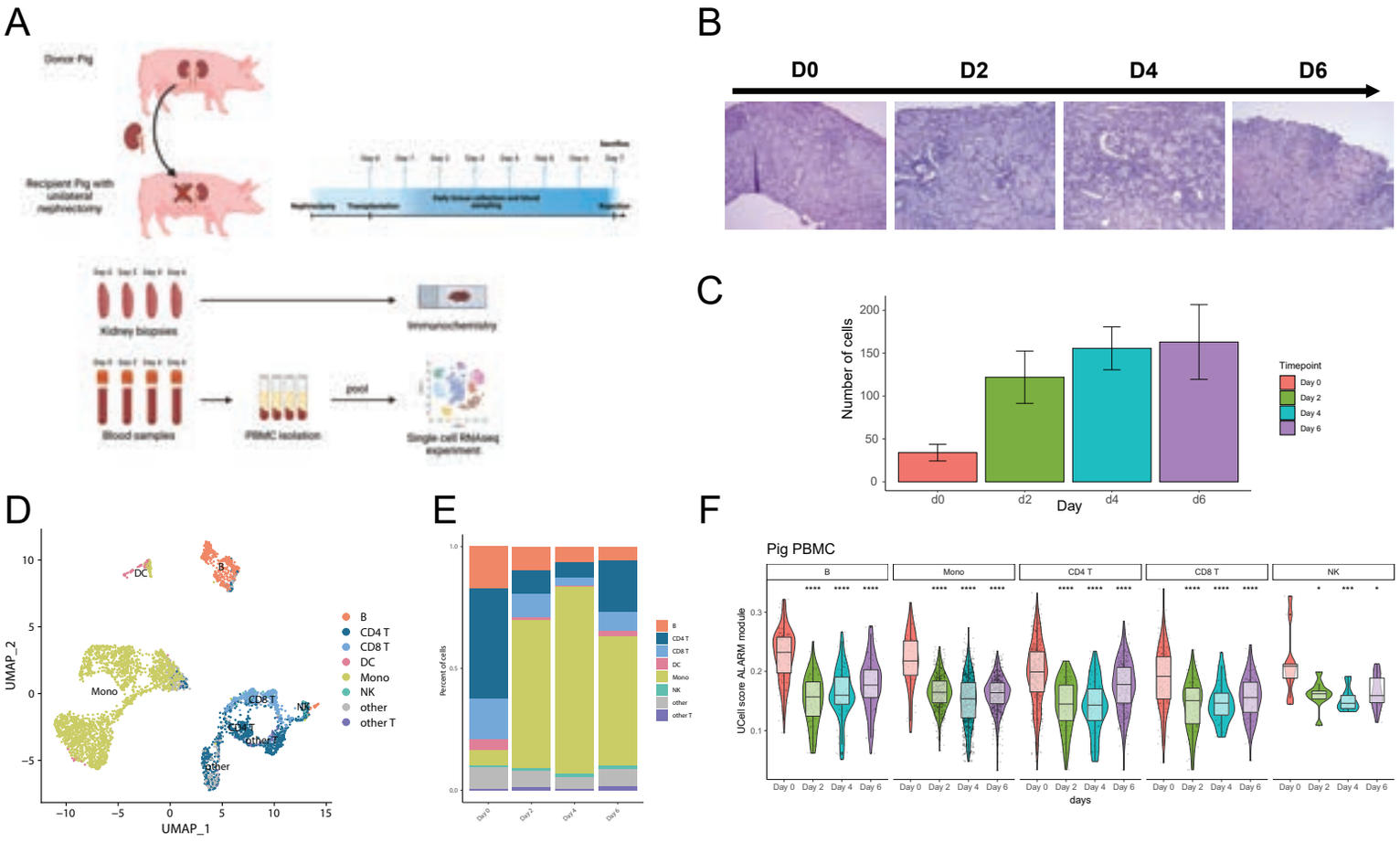
A
Donor Pig
Recipient Pig with unilateral nephrectomy
Kidney biopsies
Immunochemistry
Blood samples
PBMC isolation
pool
Single cell RNAseq experiment
B
D0
D2
D4
D6
C
Number of cells
Day
d0
d2
d4
d6
Timepoint
Day 0
Day 2
Day 4
Day 6
D
UMAP_1
UMAP_2
B
CD4 T
CD8 T
DC
Mono
NK
other
other T
E
Percent of cells
F
Pig PBMC
B
Mono
CD4 T
CD8 T
NK
UCell score ALARM module
days

Supp. Figure 3

A

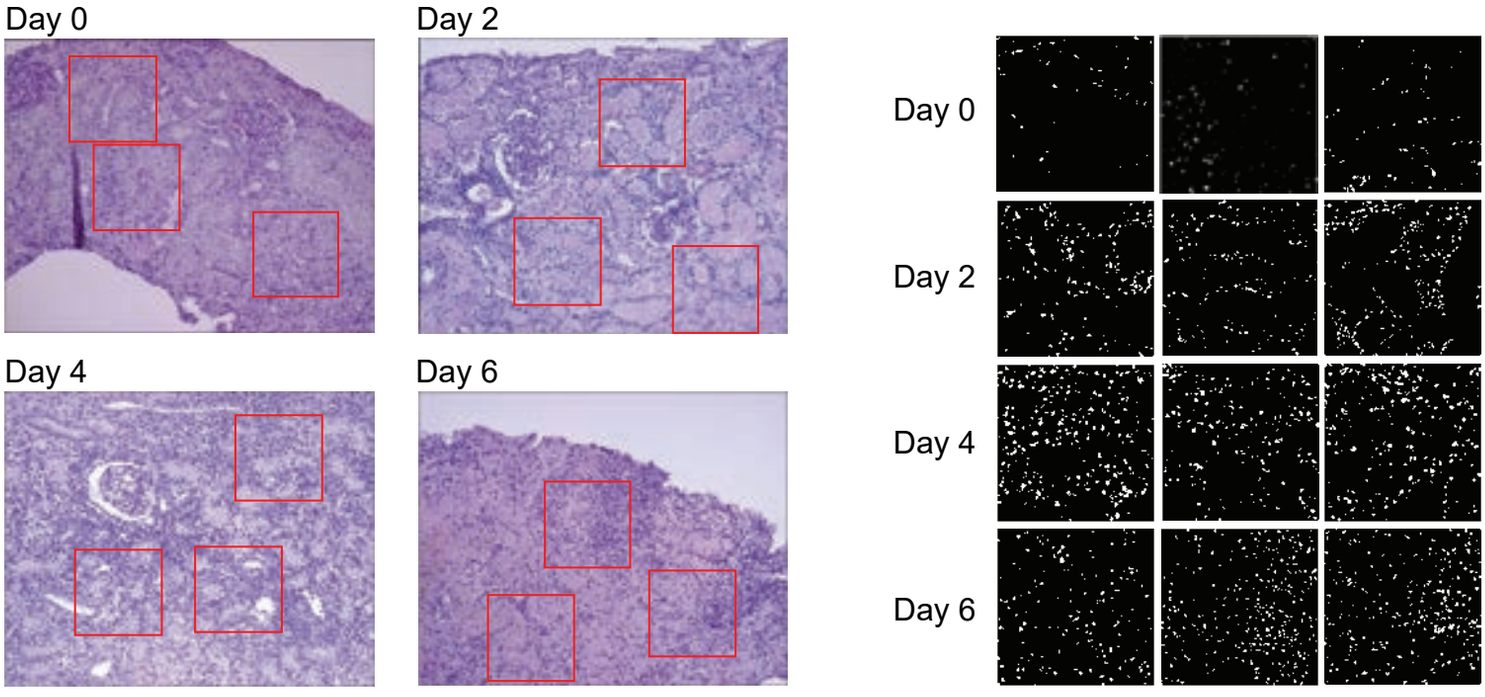

B

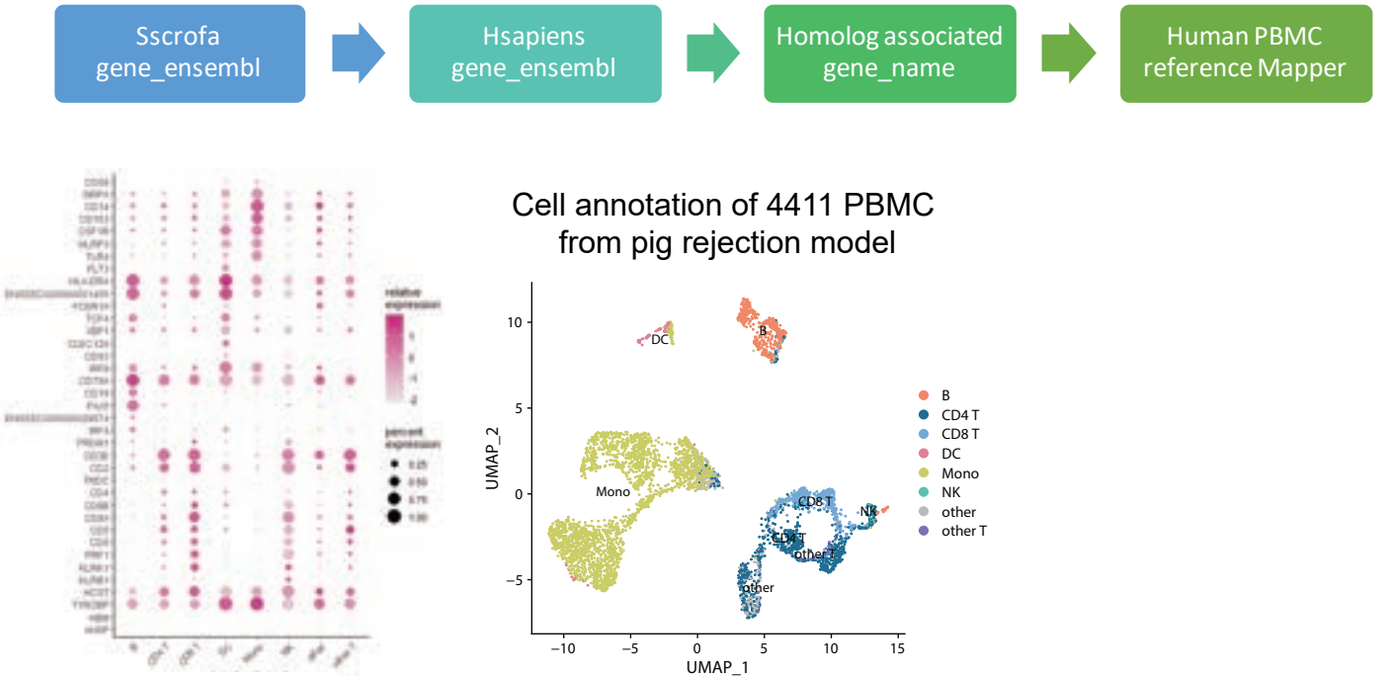

Figure 4

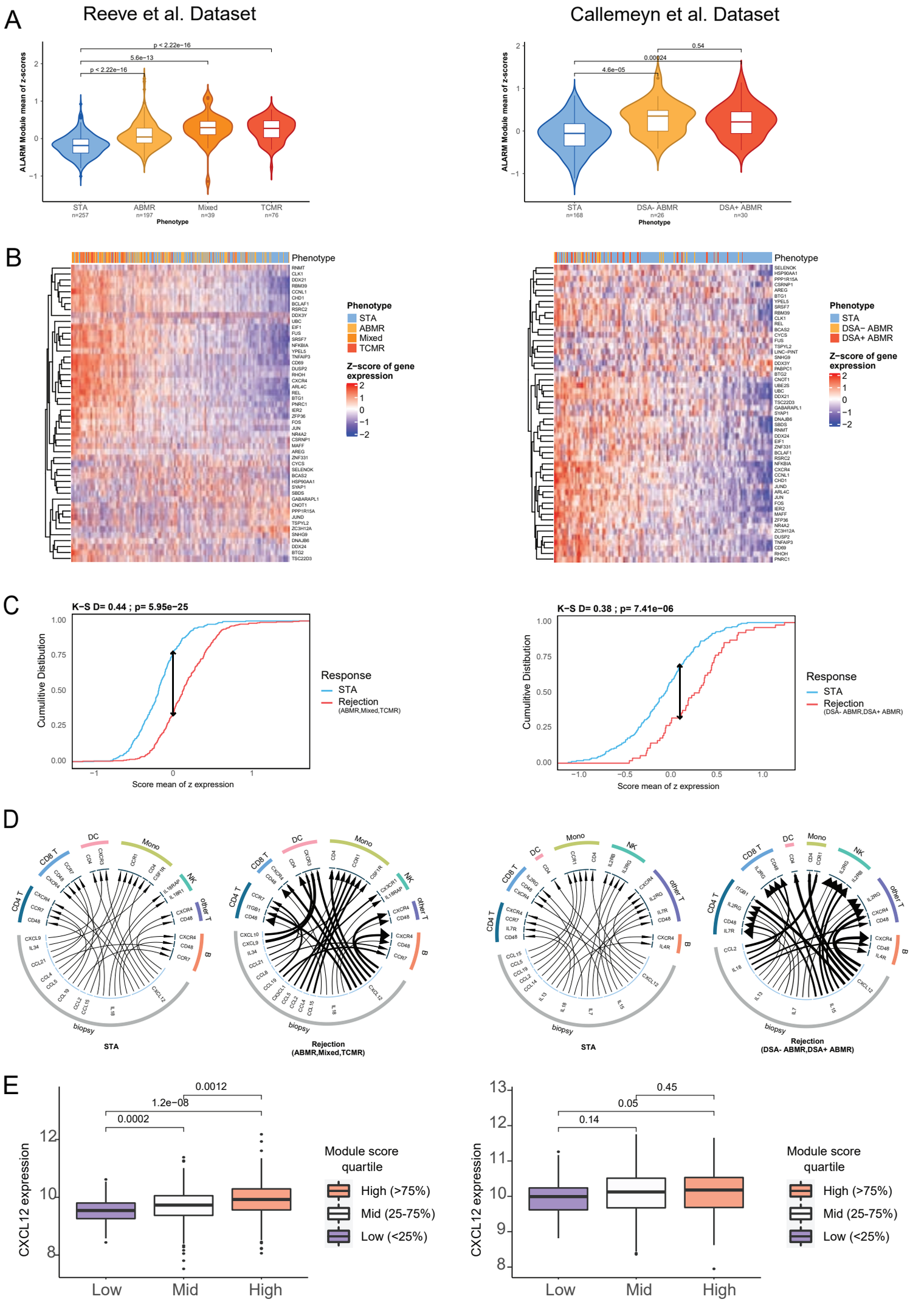
A
Reeve et al. Dataset
Callemeyn et al. Dataset
ALARM Module mean of z-scores
p < 2.22e−16
5.6e−13
p < 2.22e−16
4.6e−05
0.00024
0.54
STA n=257
ABMR n=197
Mixed n=39
TCMR n=76
STA n=168
DSA- ABMR n=26
DSA+ ABMR n=30
Phenotype
B
Phenotype
STA
ABMR
Mixed
TCMR
DSA− ABMR
DSA+ ABMR
Z−score of gene expression
C
K−S D= 0.44 ; p= 5.95e−25
K−S D= 0.38 ; p= 7.41e−06
Cumulitive Distibution
Score mean of z expression
Response
STA
Rejection (ABMR,Mixed,TCMR)
Rejection (DSA- ABMR,DSA+ ABMR)
D
DC
Mono
CD8 T
NK
CD4 T
other T
B
biopsy
STA
Rejection (ABMR,Mixed,TCMR)
Rejection (DSA- ABMR,DSA+ ABMR)
E
CXCL12 expression
0.0012
1.2e−08
0.0002
0.45
0.05
0.14
Low
Mid
High
Module score quartile
High (>75%)
Mid (25-75%)
Low (<25%)

Figure 5

A

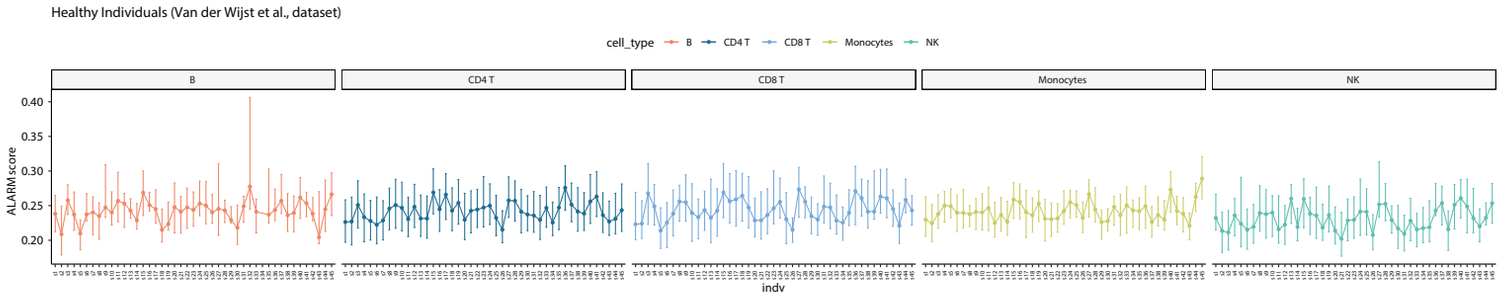

B

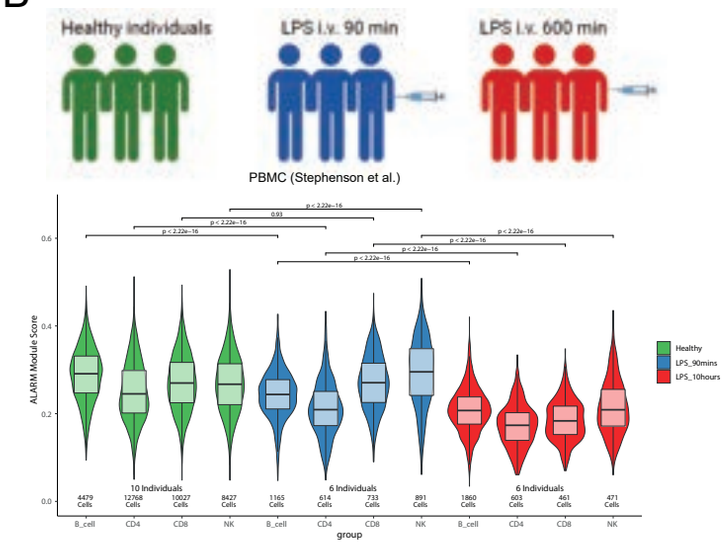

C

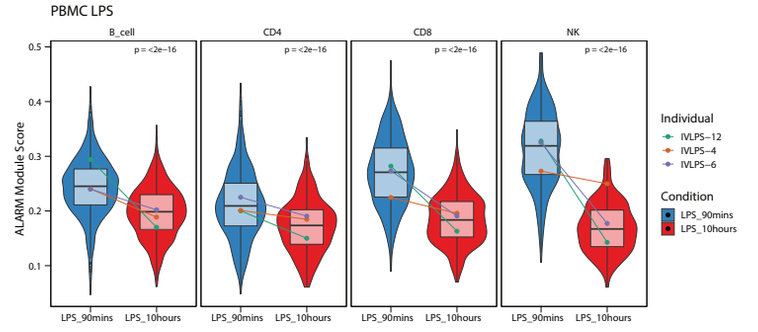

D

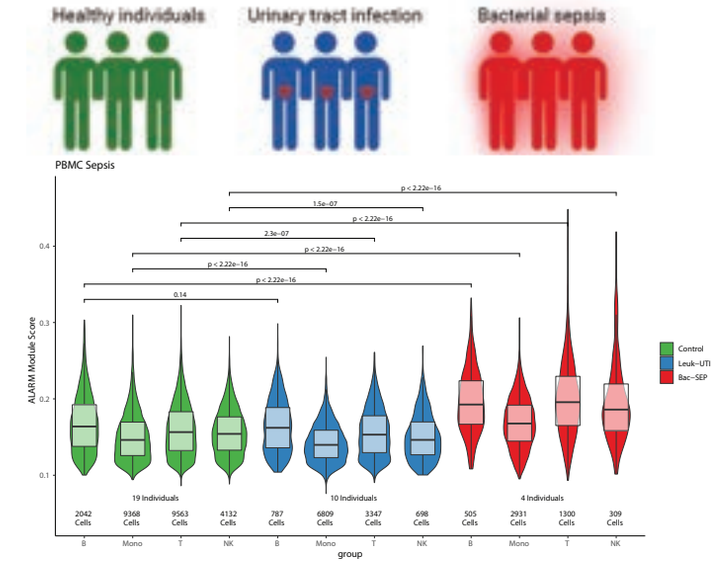

E

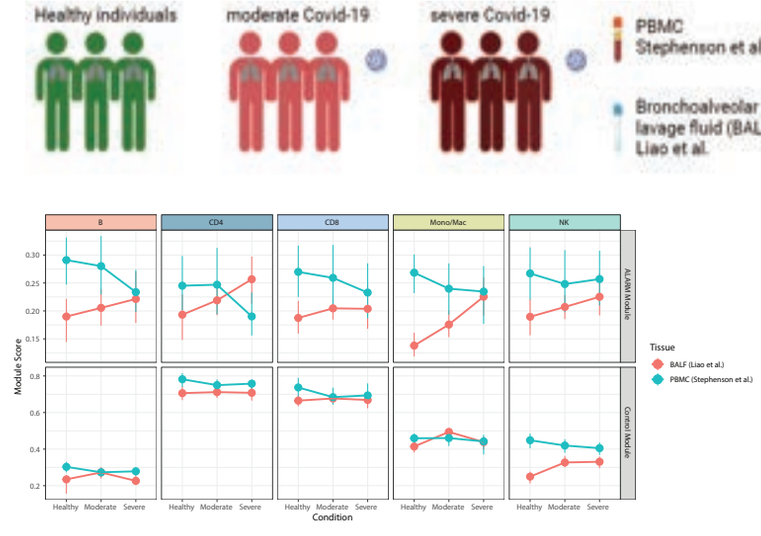

Supp. Figure 5

A

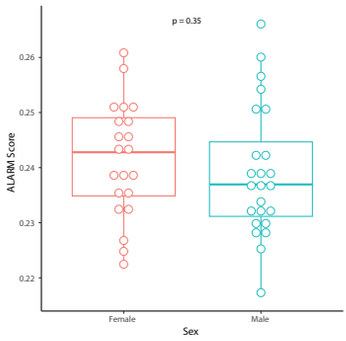

B

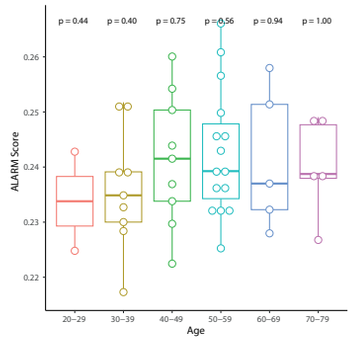

Figure 6

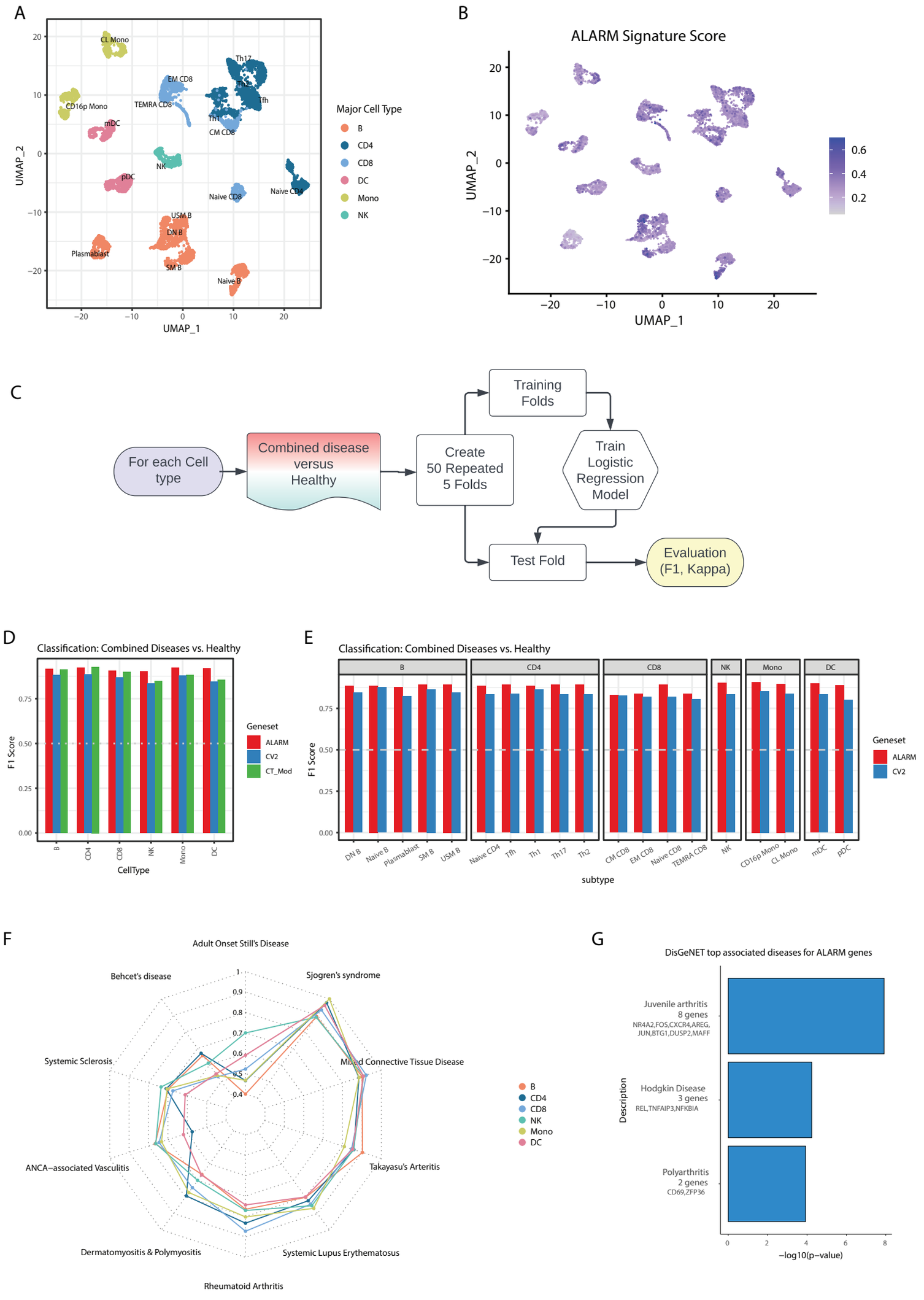
A
CL Mono
Th17
EM CD8
Th2
Tfh
CD16p Mono
TEMRA CD8
mDC
Th1
CM CD8
NK
pDC
Naive CD8
Naive CD4
USM B
DN B
Plasmablast
SM B
Naive B
UMAP_1
UMAP_2
Major Cell Type
B
CD4
CD8
DC
Mono
NK
B
ALARM Signature Score
UMAP_1
UMAP_2
C
For each Cell type
Combined disease versus Healthy
Create 50 Repeated 5 Folds
Training Folds
Train Logistic Regression Model
Test Fold
Evaluation (F1, Kappa)
D
Classification: Combined Diseases vs. Healthy
F1 Score
CellType
Geneset
ALARM
CV2
CT_Mod
E
Classification: Combined Diseases vs. Healthy
F1 Score
subtype
Geneset
ALARM
CV2
F
Adult Onset Still's Disease
Sjogren's syndrome
Mixed Connective Tissue Disease
Takayasu's Arteritis
Systemic Lupus Erythematosus
Rheumatoid Arthritis
Dermatomyositis & Polymyositis
ANCA–associated Vasculitis
Systemic Sclerosis
Behcet's disease
B
CD4
CD8
NK
Mono
DC
G
DisGeNET top associated diseases for ALARM genes
Juvenile arthritis
8 genes
NR4A2,FOS,CXCR4,AREG,
JUN,BTG1,DUSP2,MAFF
Hodgkin Disease
3 genes
REL,TNFAIP3,NFKBIA
Polyarthritis
2 genes
CD69,ZFP36
Description
−log10(p−value)

Supp. Figure 6

A

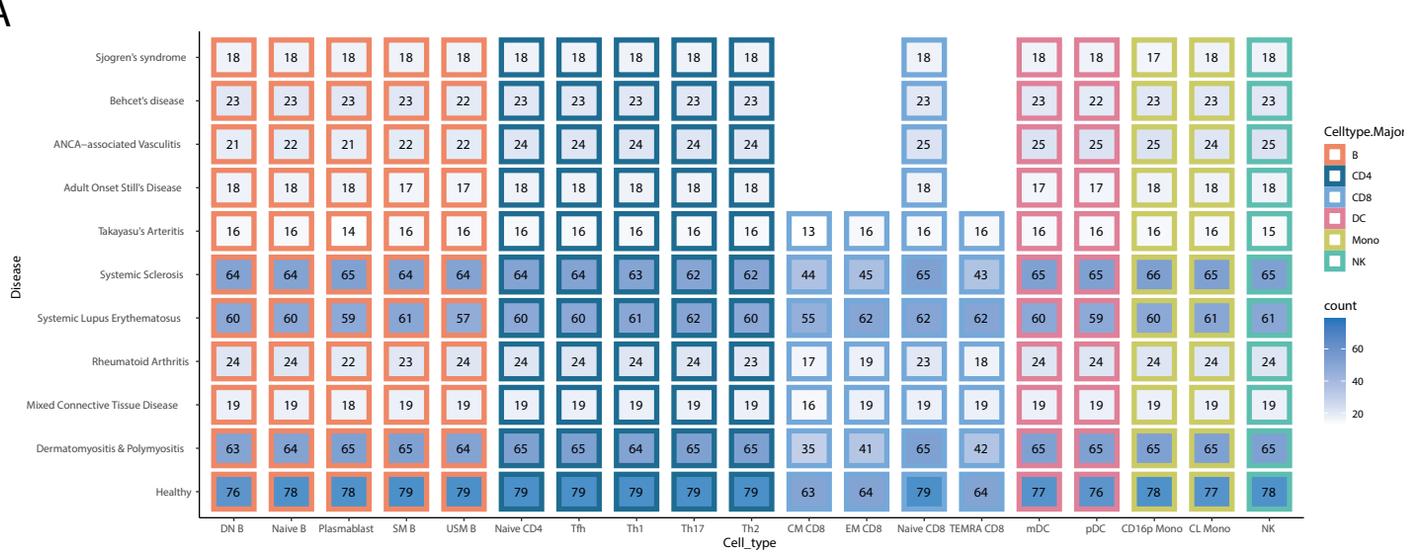

B

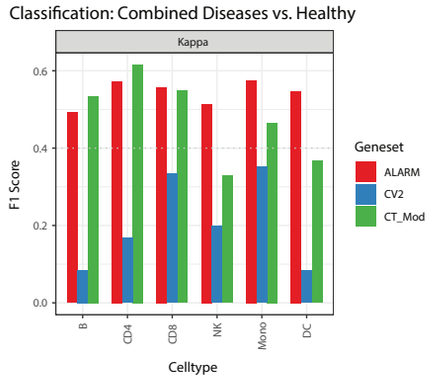

C

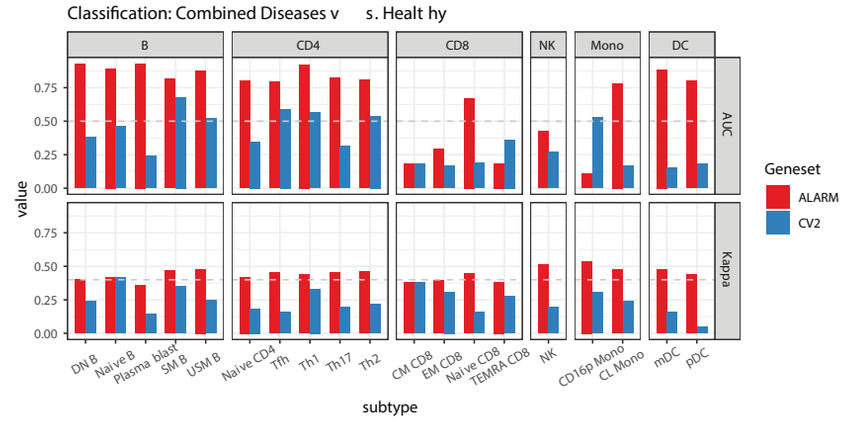

D

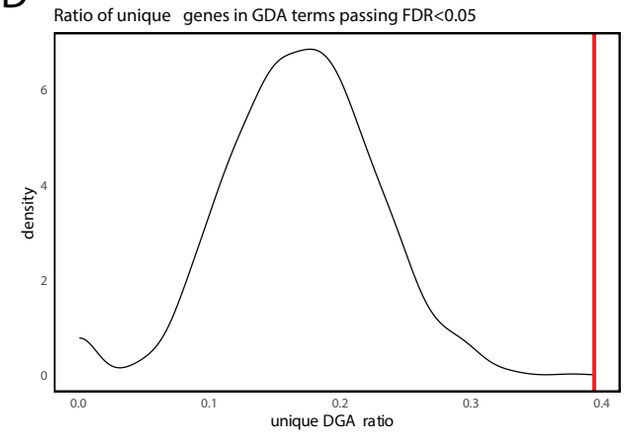

Model

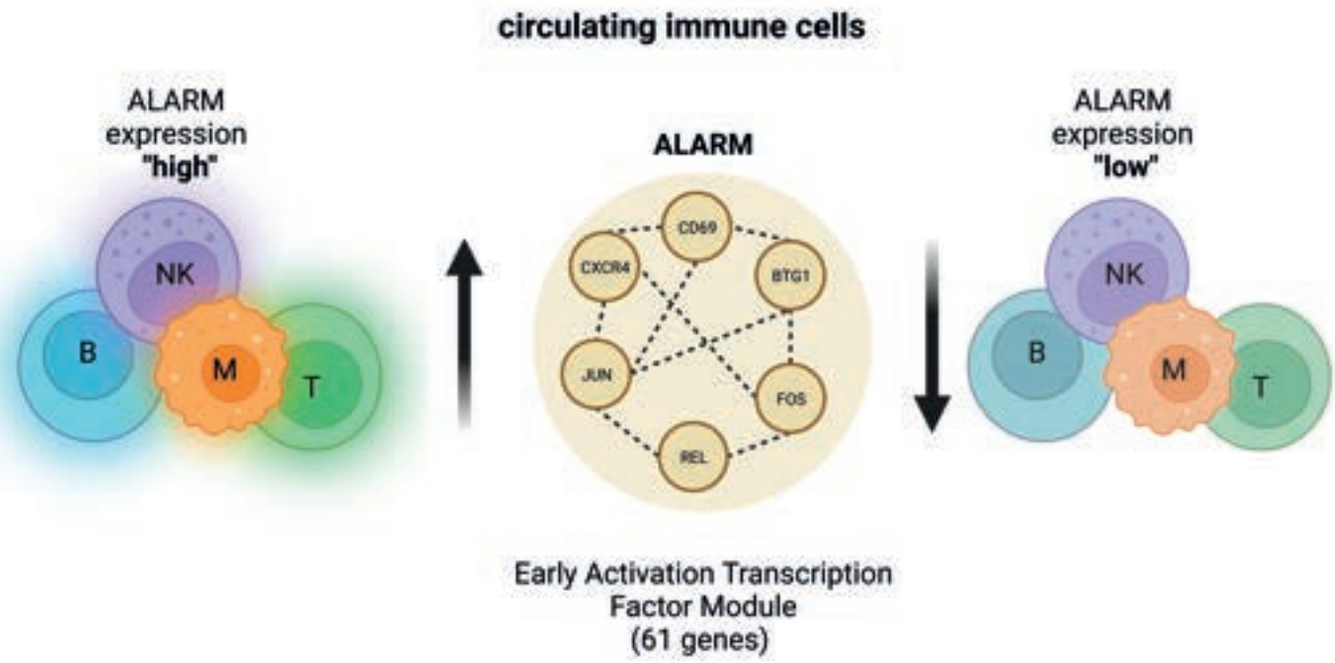
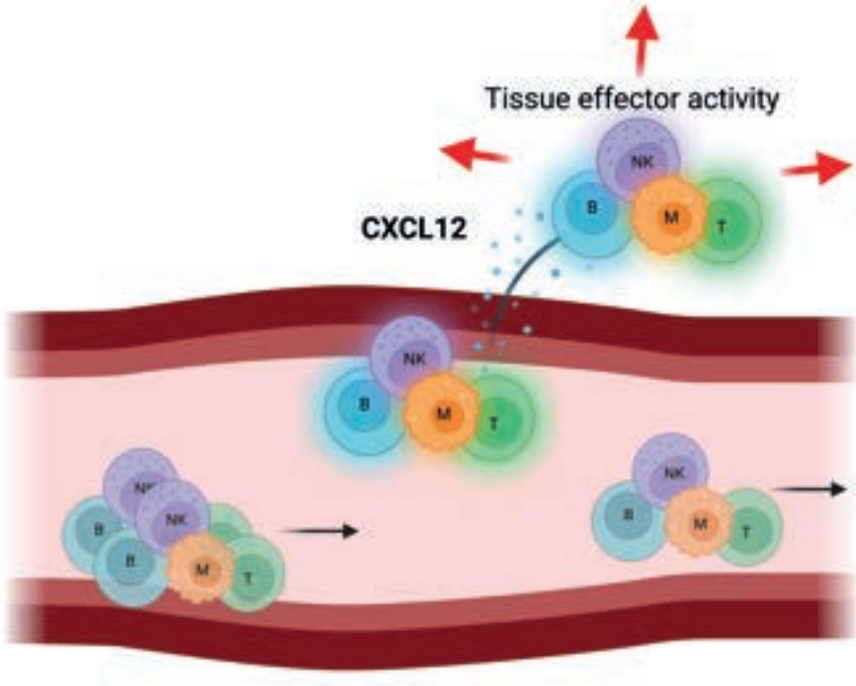
- Peripheral blood mononuclear cells express ALARM at different levels
- ALARM cells are depleted in the blood in response to tissue infection & inflammation
- ALARM cells increase at site of infection and inflammation
- Recruitment of ALARM is associated to CXCL12 expression in the tissue
- ALARM cells are implicated across a wide variety of immune diseases
- ALARM genes are strong predictors of immune mediated diseases